



**Verification of an
ADER-DG method**

C. Pelties et al.

Verification of an ADER-DG method for complex dynamic rupture problems

C. Pelties¹, A.-A. Gabriel¹, and J.-P. Ampuero²

¹Department of Earth and Environmental Sciences, Geophysics Section,
Ludwig-Maximilians-Universität, Munich, Germany

²Seismological Laboratory, California Institute of Technology, Pasadena, California, USA

Received: 8 November 2013 – Accepted: 12 November 2013 – Published: 28 November 2013

Correspondence to: C. Pelties (pelties@lmu.de)

Published by Copernicus Publications on behalf of the European Geosciences Union.

Title Page

Abstract

Introduction

Conclusions

References

Tables

Figures



Back

Close

Full Screen / Esc

Printer-friendly Version

Interactive Discussion



Abstract

We present thorough benchmarking of an arbitrary high-order derivative Discontinuous Galerkin (ADER-DG) method on unstructured meshes for advanced earthquake dynamic rupture problems. We validate the method in comparison to well-established numerical methods in a series of verification exercises, including dipping and branching fault geometries, heterogeneous initial conditions, bi-material cases and several rate-and-state friction constitutive laws. We show that the combination of meshing flexibility and high-order accuracy of the ADER-DG method makes it a competitive tool to study earthquake dynamics in complicated setups.

1 Introduction

The combined simulation of dynamic fault rupture and seismic wave propagation is a useful tool to gain insight into the poorly constrained processes of earthquake faulting. Dynamic rupture modeling aims to understand the underlying physics governing earthquakes and may be incorporated in physics-based seismic hazard assessment and strong motion prediction in preparation of future, possibly devastating, events (Ely et al., 2010; Harris et al., 2011; Roten et al., 2011).

Recent advances in dynamic rupture simulations furthered our understanding of the earthquake cycle in the Parkfield region (Barbot et al., 2012), the influence of low velocity fault zones (Huang and Ampuero, 2011) and off-fault plasticity (Templeton and Rice, 2008; Ma and Andrews, 2010; Gabriel et al., 2013) on the dynamics of the fracture process, mechanisms to generate pulse-like and supershear earthquakes and their consequences (Dunham, 2007; Daub et al., 2010; Gabriel et al., 2012) and the interaction of fault zone branches (Oglesby et al., 2003; Bhat et al., 2007; DeDontney et al., 2011). Dynamically consistent predictions of strong ground motion excitation in earthquake scenarios have been pushing computational performance to the petaflop scale (Cui et al., 2010; Zhou et al., 2013).

GMDD

6, 5981–6034, 2013

Verification of an ADER-DG method

C. Pelties et al.

Title Page

Abstract

Introduction

Conclusions

References

Tables

Figures

◀

▶

◀

▶

Back

Close

Full Screen / Esc

Printer-friendly Version

Interactive Discussion



Verification of an ADER-DG method

C. Pelties et al.

Title Page

Abstract

Introduction

Conclusions

References

Tables

Figures

◀

▶

◀

▶

Back

Close

Full Screen / Esc

Printer-friendly Version

Interactive Discussion



Nevertheless, despite the current achievements, the numerical simulation of the rupture process and its implementation into elastodynamics solvers poses challenges. For instance, the natural discontinuity of physical variables across the fault interface has to be approximated accurately and accounted for by the computational mesh. Furthermore, the dynamic rupture implementation in many numerical methods, such as finite difference, finite element and spectral element methods, suffers from spurious high-frequency oscillations, that may counteract the non-linear wave and rupture interaction in dynamic earthquake simulations and potentially contaminate the solution over all space-time scales (Duan and Day, 2008). Thus, numerical regularization, artificial attenuation or smoothing is usually necessary to suppress high-frequency numerical noise with spatial scale near the resolution limit of the mesh. Such artificial damping mechanisms, as for example the deployment of a thin layer of Kelvin–Voigt viscous material surrounding the fault, e.g. Ampuero (2008); Day et al. (2005); Dalguer and Day (2007), are not completely satisfying. The physical solution is not necessarily insensitive to the precise parametrization of the added damping, which interferes with the actual physics of interest, for example by slowing down the rupture propagation (Andrews, 2005) and smoothing out small scale features, and may also reduce the time step length and thus increase the computational effort considerably.

Realistic earthquake scenario simulations would ideally cover a frequency range relevant for engineering applications (up to 20 Hz), and include geological models spanning hundreds of kilometers consisting of complicated fault geometries, topography, oceans and low velocity sedimentary basins. Simultaneously, small-scale high resolution is required to resolve the frictional sliding in the so-called cohesive zone at the rupture tip with a sufficient number of computational nodes or elements, e.g. at scales down to meters in case of slip-weakening constitutive behavior (Day et al., 2005). The constitutive laws describing the frictional sliding of faults originate in laboratory experiments carried out on much smaller scales than in natural setups (Dieterich, 1978; Ohnaka and Mogi, 1982; Di Toro et al., 2005). While it is still uncertain how to extrapolate fault constitutive properties from laboratory to natural scales, testing the large

Verification of an ADER-DG method

C. Pelties et al.

Title Page

Abstract

Introduction

Conclusions

References

Tables

Figures

◀

▶

◀

▶

Back

Close

Full Screen / Esc

Printer-friendly Version

Interactive Discussion



scale implications of laboratory friction poses an enormous computational challenge. Additionally, the propagation of small wavelengths over large distances accumulates numerical dispersion and diffusion errors and favors a high-order accurate discretization. Another challenge for dynamic rupture simulations are large uncertainties in physical initial conditions and fault constitutive parameters. The rupture evolution depends strongly on model parameters such as initial background stresses, nucleation procedure and frictional properties. Forward modeling of dynamic rupture can support the search for proper friction models and model parameters (Cochard and Madariaga, 1994; Day et al., 1998; Aochi et al., 2003; Kaneko et al., 2008; Brietzke et al., 2009).

In order to avoid additional errors that interfere with the physical problem accurate numerical methods that produce reliable results are desirable. Furthermore, computational efficiency, parallelization and high scalability are crucial demands for numerical methods simulating realistic earthquake scenarios.

In this paper, we present a thorough verification study of the software SeisSol (Käser and Dumbser, 2006; Dumbser and Käser, 2006), a high-order derivative Discontinuous Galerkin (ADER-DG) method on unstructured meshes, for advanced dynamic rupture problems (de la Puente et al., 2009; Pelties et al., 2012). In contrast to the well verified and validated simulation of seismic wave propagation, the verification process of spontaneous rupture dynamic simulations suffers from missing analytical reference solutions. Therefore, we verify the performance of the ADER-DG method in the benchmark suite established by the Southern California Earthquake Center (SCEC) (Harris et al., 2009; Harris et al., 2011). All simulation results presented here are available at <http://sceccdata.usc.edu/cvws/>. To this end, we cover many aspects important in realistic faulting setups, including dipping and branching fault geometries, bi-material cases, heterogeneous initial conditions and different formulations of rate-and-state friction laws.

Our results demonstrate the benefits of SeisSol for dynamic rupture and ground motion simulations in realistic settings. Importantly, we confirm the lack of systematic numerical artifacts in advanced faulting setups, as reported for the basic example of

a planar fault embedded in a homogeneous full space (SCEC Test Case TPV3) by Pelties et al. (2012).

2 Numerical method

de la Puente et al. (2009) and Pelties et al. (2012) presented a new and alternative numerical scheme for the simulation of earthquake faulting. The underlying solver for the wave propagation is an ADER-DG method (Käser and Dumbser, 2006; Dumbser and Käser, 2006) with high order accuracy in space and time based on tetrahedral element discretization. Between any two elements information is exchanged via numerical fluxes. We briefly outline the algorithm used to evaluate the friction law in Appendix A and extend this approach to faulting at dissimilar material contacts. For further details on the concept, the reader is referred to de la Puente et al. (2009) and Pelties et al. (2012). The software package SeisSol provides pre- and post-processing tools including interfaces to external mesh generators and a mesh partitioning concept based on METIS (Karypis and Kumar, 1998).

The use of a tetrahedral element discretization leads to rapid and automatized mesh generation that can be readily aligned to complex geometrical features. Furthermore, the possibility of mesh refinement is advantageous for dynamic rupture problems as the mesh resolution can be adapted to areas of interest, such as the fault plane or areas of complex topography, whereas the mesh size can be coarsened with increasing distance from the fault to reduce the computational cost. Note that no artificial reflections due to mesh coarsening are observed (de la Puente et al., 2009).

In contrast to the typically applied traction at split-node approach (Andrews, 1999; Day et al., 2005; Dalguer and Day, 2007), ADER-DG solves the frictional sliding via the inverse Riemann problem (Toro, 1999; LeVeque, 2002), in which the exact solution is modified to incorporate frictional boundary conditions. Solving the inverse Riemann problem inherits the favorable numerical properties from the exact Riemann solver or Godunov flux. The numerical properties of the ADER-DG algorithm are extremely

Verification of an ADER-DG method

C. Pelties et al.

Title Page

Abstract

Introduction

Conclusions

References

Tables

Figures

◀

▶

◀

▶

Back

Close

Full Screen / Esc

Printer-friendly Version

Interactive Discussion



**Verification of an
ADER-DG method**

 C. Pelties et al.

[Title Page](#)
[Abstract](#)
[Introduction](#)
[Conclusions](#)
[References](#)
[Tables](#)
[Figures](#)
[⏪](#)
[⏩](#)
[◀](#)
[▶](#)
[Back](#)
[Close](#)
[Full Screen / Esc](#)
[Printer-friendly Version](#)
[Interactive Discussion](#)


sensitive to the choice of flux function. In particular, our implementation using an up-wind flux introduces a very selective numerical dissipation, as already discussed in Pelties et al. (2012). The dissipation increases with increasing frequencies and is stronger beyond a cut-off frequency that depends on the mesh size h and on the order of accuracy \mathcal{O} . The cut-off frequency is expected to be inversely proportional to the travel time of S waves over a typical grid spacing $\sim h/\mathcal{O}/c_s$. Higher frequency modes are subdued while the physically meaningful lower frequencies are minimally affected. This is advantageous for dynamic rupture simulations: spurious high-frequency oscillations are not generated in the first place and, thus, no additional damping procedures need to be applied.

For consistency, we compare our results to the well-established software FaultMod (Barall, 2009) throughout this paper. FaultMod is a finite element (FE) code designed specifically for constructing physics-based models of fault systems which involve complex 3-D geometry and 3-D variation of material properties. The implementation of fault friction is based on the traction-at-split-nodes method (Andrews, 1999). Faults are represented using common and differential nodes, which have a non-diagonal mass matrix. Also, FaultMod uses an implicit time stepping algorithm, where displacement, velocities, and acceleration are computed simultaneously. The method implements Newmark damping (Hughes, 2000) and an optional thin viscous layer surrounding the fault zone (Day et al., 2005; Dalguer and Day, 2007) to suppress unwanted high-frequency oscillations.

In Sect. 7 we furthermore show a comparison of our results with other high-order dynamic rupture codes based on a variety of numerical methods.

3 Dip-slip fault with depth dependent background stress conditions

Many studies of earthquake source physics have focused on purely strike-slip faulting. Nevertheless, subduction zone settings, in which most of the seismic energy was released over the last century (Pacheco and Sykes, 1992), are dominated by dip-slip

Verification of an ADER-DG method

C. Pelties et al.

Title Page

Abstract

Introduction

Conclusions

References

Tables

Figures

◀

▶

◀

▶

Back

Close

Full Screen / Esc

Printer-friendly Version

Interactive Discussion



faults, as well as many other fault types exhibit dipping components. The asymmetric geometry of dipping faults is of particular interest, since it results in asymmetric near-source ground motion (Oglesby et al., 1998). Furthermore, in case of surface rupture, the arrival of the rupture front at the free surface strongly excites seismic waves (Madariaga, 2003) and the dynamic rupture evolution interacts with reflected waves from the free-surface (Huang et al., 2013). Accurately reproducing these effects in numerical simulations poses challenges in terms of mesh generation and numerical stability.

We model nucleation followed by spontaneous rupture on a 60° dipping normal fault reaching a free surface in a homogeneous half-space. Subshear (SCEC Test Case TPV10) and supershear (SCEC Test Case TPV11) conditions are parameterized by varying the value of the static coefficient of friction. Rupture is initiated by increasing the background dip-direction shear stress until a value larger than the static yield strength in a pre-defined nucleation patch is reached. For the entire fault plane, including the nucleation patch, both the initial fault normal stress and the initial along-dip shear-stress increase linearly with down-dip distance. In order to accurately sample the initial stress and material parameters we assign individual values to every Gaussian integration point. Slip-weakening friction and elastic off-fault yielding are assumed. All simulation parameters are summarized in Table 1.

We compare the ADER-DG $\mathcal{O}5$ solution using an edge length of 200 m to the finite element method FaultMod of Barall (2009) with an edge length of 100 m and $\mathcal{O}2$. Our mesh was gradually coarsened to maximum edge lengths of 5 km far away from the fault to concentrate numerical costs where needed. Figure 1a depicts the asymmetric unstructured mesh discretizing the computational domain and a snapshot of the absolute particle velocity on the dipping fault plane during the simulation.

The ADER-DG on-fault receivers, such as the station shown in Fig. 1b and c, show generally an excellent agreement with the FEM reference solution, despite the asymmetric unstructured mesh surrounding the fault discontinuity in the ADER-DG case.

Nevertheless, the already damped finite element solution still shows signs of high-frequency oscillations in slip-rate amplitudes.

The development of a supershear daughter pulse in TPV11, caused by stress concentration ahead of the sub-shear rupture front (Dunham, 2007), is equally well captured, as shown in Fig. 2. The contour plot in Fig. 2a captures the boost in rupture velocity after supershear transition. We also point out the normal stress variation (Fig. 2b) caused by the interaction of the non-vertical fault with the Earth's free surface as investigated e.g. by Rudnicki and Wu (1995), Dalguer et al. (2001), Ma and Archuleta (2006), Andrews et al. (2007) and Ma and Beroza (2008). Interestingly, we see differences in the evolution of stresses after 10 s: the FEM solution reaches higher normal and along-dip shear stresses leading to a slight difference in slip rate. This might be due to free surface effects, differently handled by both methods.

Effects of strong ground shaking due to free surface interaction, as well as an asymmetry between foot wall and hanging wall can be observed in Fig. 3. Larger ground motions on the hanging wall than on the footwall are observed in natural earthquakes, e.g. Abrahamson and Somerville (1996), and can be related to normal stress variation inducing strength drop variations. The agreement between ADER-DG and FEM regarding the synthetic ground motions in the vicinity of the fault is near-perfect.

4 Heterogeneous background stress fields

Tectonic loading plays a fundamental role in earthquake source dynamics and controls the size of an earthquake. Stress heterogeneities could potentially influence nucleation and arrest of a rupture (Day, 1982; Boatwright and Quin, 1986; Oglesby and Day, 2002; Ampuero et al., 2006). An unanswered question is how small scale fluctuations of the prescribed initial stress fields modulate the rupture process. As stresses in the Earth's interior can not be measured directly, dynamic rupture simulations represent a proper tool to analyze the impact of small scale stress variations.

Verification of an ADER-DG method

C. Pelties et al.

Title Page

Abstract

Introduction

Conclusions

References

Tables

Figures



Back

Close

Full Screen / Esc

Printer-friendly Version

Interactive Discussion



GMDD

6, 5981–6034, 2013

Verification of an
ADER-DG method

C. Pelties et al.

Title Page

Abstract

Introduction

Conclusions

References

Tables

Figures

◀

▶

◀

▶

Back

Close

Full Screen / Esc

Printer-friendly Version

Interactive Discussion



The SCEC benchmark problems TPV16 and 17 focus on the modeling of dynamic rupture under heterogeneous initial stress conditions. Here, we consider only TPV17, as TPV16 is very similar. The randomly generated heterogeneous initial stress conditions and the frictional parameters are given by a pre-defined input file. The setup contains a planar strike-slip fault embedded in a linear elastic medium with wave speeds specified in Table 2. Linear slip-weakening governs the frictional sliding. The nucleation method is achieved through high stress values in the hypocentral region with an approximated radius of 1 km and low D_c values in the hypocentral region with an approximated radius of 4 km. Furthermore, the friction coefficient is set to the lower dynamic friction coefficient following a pre-defined time dependent function that creates an expanding circular region of forced rupture propagating away from the hypocenter.

The effect of heterogeneous initial stresses on dynamic rupture propagation needs particular scrutiny in methods based on high-order discretizations, which work more efficiently on large elements (Käser et al., 2008). Even if the dispersion requirements are sufficiently addressed by large elements and a high-order approach, yet another issue is the correct sampling of the given initial stress and friction data on the fault. Pelties et al. (2010) attempted to define rules to respect material properties of a complex geological medium correctly, but we are not aware of a study addressing this issue for the initial stress conditions of a dynamic rupture simulation. As introduced in Sect. 2 and Appendix A, in the case of slip occurring at the fault we modify flux functions in accordance with the Coulomb failure criterion. The fault plane is hereby always located at the interface between two adjacent elements. These flux functions are integrated on $(N + 2)^2$ Gaussian integration points (GP) irregularly distributed across each triangular element face, where N is the polynomial degree of the basis functions. We assign initial values of friction coefficient, critical slip distance, stress or other parameters to every Gaussian integration point at the fault interface individually.

In this particular example we use a trilinear interpolation algorithm to map the given gridded data on the irregularly distributed GPs. In this way, the smallest possible scale of the numerical method is exploited without decreasing the element size and

thus sub-element resolution is enabled. A typical resolution of element edge length $h = 200$ m and $\mathcal{O}4$ is applied in order to test if our proposed sub-sampling scheme is sufficient to capture the initial stress values and frictional parameters. Note that again mesh coarsening with distance to the fault is applied.

Figure 4 demonstrates the complexity of the rupture propagation caused by the small-scale heterogeneous background stress. Considering the given complexity of the model we find good agreement between the two compared methods. The good match can also be confirmed by Figs. 5 and 6 where the time series of two receivers located on the fault plane are shown. Figure 7 shows a snapshot of the horizontal component of slip rate at 5.5 s across the entire fault plane and indicates the location of the receiver of Fig. 5. In Fig. 5c we can identify a sharp feature at ~ 5.5 s in the horizontal slip rate. From Fig. 7, we can identify this sharp feature as an interface wave (Dunham, 2005). Reflection at the free surface causes a healing front which passes the receiver after the rupture front and is followed immediately by a secondary slip rate peak. Note that the amplitude of the latter peak even exceeds the peak slip rate of the primary rupture front. At other positions of the fault, the healing mechanism caused by an interface wave is not as pronounced. We argue that this effect is physically correct within the limits of the provided model as it is also simulated by other numerical methods at high resolution (see the data provided by the SCEC Code Comparison tool). We emphasize the remarkable accuracy of the ADER-DG solver allowing to resolve these small scale features with a relatively large element edge length of $h = 200$ m. Therefore, we conclude the approach of sampling the background model by the Gaussian integration points works sufficiently to reach agreement to the well established and tested method FaultMod (FEM).

5 Fault branching

Fault branching has been observed in natural events, e.g. Schwartz et al. (2012). Incorporating the possible propagation of an earthquake rupture from one fault to another

Title Page

Abstract

Introduction

Conclusions

References

Tables

Figures

◀

▶

◀

▶

Back

Close

Full Screen / Esc

Printer-friendly Version

Interactive Discussion



Verification of an ADER-DG method

C. Pelties et al.

Title Page

Abstract

Introduction

Conclusions

References

Tables

Figures

◀

▶

◀

▶

Back

Close

Full Screen / Esc

Printer-friendly Version

Interactive Discussion



may lead to earthquake scenarios involving very different magnitudes, which would be of crucial importance in a seismic hazard analysis. However, the role of fault branching in earthquake dynamics is poorly understood. On the one hand, realistic simulations would need reliable information about the fault geometry, on the other hand, the theoretical analysis of fault branching mechanisms is reduced to simplified scenarios. Defining mathematical predictions for dynamic rupture propagation at the junction point of main fault and branch turns out to depend sometimes on the specific boundary conditions assumed at the junction (DeDontney et al., 2011).

To verify the performance of the ADER-DG algorithm on a branching fault system we discuss here SCEC's Test Cases TPV14 and TPV15 benchmarks. The geometrical setup contains two vertical, planar, strike-slip faults; a main fault and a branch fault in a 30° angle. The faults reach the Earth's surface. In TPV14 the initial stress conditions determine the fault system as right-lateral and in TPV15 as left-lateral. Here, we focus on TPV15.

The line where main fault and branch fault intersect is referred to as junction point. However, as specified in the benchmark description, the branch fault should not fully reach the junction point. A small gap with the length of one grid spacing between the two faults is prescribed. This way, a rupture nucleated on the main fault can propagate freely onto the right side of the main fault passing the junction point, but the rupture must jump the distance of one grid spacing to propagate onto the branch fault. Since our method is able to model both the gap between main and branch fault as well as the setup without gap, we address both cases and discuss the differences in the following. We note that the branching benchmark problems TPV24/25 without a gap at the junction were more recently formulated. However, in the modal ADER-DG formulation there is no solution defined exactly at the junction point, as physical solutions are only computed within the entire element and at the element edges, with exception of the vertices.

Important to notice is that we used the same mesh for the simulation with gap and for the simulation without gap. Technically, this is achieved by accounting for the

**Verification of an
ADER-DG method**

 C. Pelties et al.

[Title Page](#)
[Abstract](#)
[Introduction](#)
[Conclusions](#)
[References](#)
[Tables](#)
[Figures](#)
[◀](#)
[▶](#)
[◀](#)
[▶](#)
[Back](#)
[Close](#)
[Full Screen / Esc](#)
[Printer-friendly Version](#)
[Interactive Discussion](#)


intersecting faults in the mesh, but simply locking a part of the branch (resembling the gap) or allow the full branch rupture (no gap). This way, all differences in the results are only due to the influence of the gap. We choose the recommended node spacing of 100 m as the gap length, although our general applied mesh resolution at the fault is $h = 300$ m. This results in a slightly higher mesh resolution of up to $h = 100$ m in the direct vicinity of the junction point. We illustrate this in the zoomed view of the junction point of a 2-D setup in Fig. 8. The different colors represent different MPI partitions for parallel computing. Fault and MPI domains can interact in arbitrary ways, e.g. intersecting perpendicular or being parallel aligned and combinations of both. Again, mesh coarsening with distance to the fault is applied. The order of accuracy in space and time is for all simulations $\mathcal{O}4$. We summarize the complete parameters in Table 3.

For comparison we employ the results of FaultMod with 100 m and 50 m node spacing. As expected, we will see that the 100 m results of FaultMod are closer to the ADER-DG solution with gap and FaultMod's 50 m results are closer to the ADER-DG without gap solution.

First, we will discuss the contour plots of the main fault in Fig. 9a and of the branch in Fig. 9b. We found very good agreement of the early rupture evaluation away from the nucleation area. Clear differences occur along the junction point at distance along strike 0 m. Whereas both FaultMod simulations stop shortly after the junction point, except some rupture at the fault bottom and at the free-surface, the ADER-DG simulation with gap continues a further along the main fault. The ADER-DG solution without gap continues only for a short distance the main fault, stops a bit earlier than the three other solutions, but shows an early rupture near the junction point. This can be linked to an earlier rupture initiation at the branch (see Fig. 9b). The rupture of the ADER-DG with gap solution starts a little bit later like the FaultMod solutions as they need to bridge the gap first. With distance along strike, the ADER-DG solution with gap propagates slower than all other solutions, however, only at the branch. Differences occur as well as at the end of the seismogenic zone and at the free-surface along the branching fault. In Fig. 10 we present the time series of the shear stresses and slip rates in strike and dip

directions at a station on the branch 9 km away from the junction point along strike and 7.5 km deep. In general, we observe a good agreement between the four solutions. Only small differences in the dip component (Fig. 10b and d) at ~ 7.5 s are visible. Since the dip component is an order of magnitude smaller than the strike component we consider this differences as not severe.

Larger differences can be observed at receivers closer to the junction point, e.g. at the main fault 2 km along strike after the junction point and in a depth of 7.5 km as shown in Fig. 11. Whereas the shear stress in dip direction (Fig. 11b) and the normal stress (Fig. 11c) are very similar, the shear stresses along-strike differ clearly for all four simulations. Here, we can observe that the 100 m results of FaultMod tend to be closer to the ADER-DG solution with gap and FaultMod's 50 m results tend to be more similar to the ADER-DG without gap solution. We argue that this is expected as the geometrical setups are more similar. In general, all receivers far away from the junction point including the off-fault receivers (not shown here) match very well and only receivers in the direct vicinity show discrepancies that can be traced back to the gap between main and branching fault. At this point, we mention that such small differences in the geometrical model might lead to a different rupture behavior if the setup is more sensitive to the geometry or the initial stress values than this SCEC test. Therefore, an insensitivity of simulations of realistic branching scenarios to gaps implemented at branching points cannot be guaranteed and we advise modelers to handle branching geometries with caution which is in agreement with results by DeDontney et al. (2011).

6 Bi-material contrast

Natural faults often separate rocks with different rheologies, e.g. Thurber et al. (2006), which leads to normal stress variations during faulting influencing dynamic rupture propagation (Harris and Day, 1997; Ampuero and Ben-Zion, 2008; Brietzke et al., 2009). Such stress perturbation could generate under certain circumstances additional propagation modes of rupture, e.g. self-sustaining pulses, and are therefore

Verification of an ADER-DG method

C. Pelties et al.

Title Page

Abstract

Introduction

Conclusions

References

Tables

Figures

◀

▶

◀

▶

Back

Close

Full Screen / Esc

Printer-friendly Version

Interactive Discussion



Verification of an ADER-DG method

C. Pelties et al.

Title Page

Abstract

Introduction

Conclusions

References

Tables

Figures

◀

▶

◀

▶

Back

Close

Full Screen / Esc

Printer-friendly Version

Interactive Discussion



of particular interest. The instantaneous response of shear stress to normal stress change at bi-material interfaces can lead to an ill-posed problem causing an instability for a wide range of elastic material contrasts, which can excite waves of all wavelengths (Adams, 1995). Furthermore, convergence through grid size reduction cannot be achieved in this case and regularization needs to be applied. Thus, we address regularization concerns in Appendix B.

Here, we concentrate on the well-posed bi-material benchmark case TPV6, which shall be performed without any form of regularization. We define a near side and a far side of the fault plane. The far side has a wave speed reduction of 60 % and a density reduction of 20 %. The fault is a planar strike-slip fault that reaches the free-surface. Frictional sliding is governed by linear slip-weakening. The exact values of the setup can be found in Table 4. The ADER-DG results are computed with $h = 200$ m and $\mathcal{O}4$ for space and time and no form of damping. FaultMod uses a 50 m grid spacing, and applies Newmark damping and a viscous layer surrounding the fault to suppress artificial oscillations.

Figure 12 shows the contour plot of the rupture front evolution. We found very good agreement of the rupture speed between the two methods. Only small differences in the arrival time occur in the dip direction.

These differences can be noted also in the time series shown in Fig. 13. This receiver is located at the near side of the fault above the nucleation zone at the free surface. Whereas the initial waves arrive at same times for both methods, the FEM solution seems to evolve slower to the peak values. Thus, the fault fails later than in the ADER-DG solution, which would explain the delay in the rupture arrival time. This effect might be caused by the damping algorithm or the viscosity layer surrounding the fault implemented in FaultMod. The general shape of the stresses and particle velocity time series are, however, very similar. Only the relatively small vertical solutions for shear stress and velocity show larger deviations as observed in Fig. 13b and e. The match of the normal components is again very good, although FaultMod computes slightly

smaller peak values (Fig. 13c and f). Note that the ADER-DG solution has only small oscillations in all produced time series.

For the sake of completeness, time series recorded at the far side of the fault, larger distance of the nucleation zone, and at same depth as the previous station are presented in Fig. 14. At this station, rupture arrival time and slip rate peak seem to match better than for the near side station above the nucleation zone. We conclude that a very good agreement can be found for the well-posed bi-material problem for ADER-DG and FaultMod.

7 Rate and state friction

The appropriate form of the constitutive law which describes the relationship between fault stress and slip along a fault plane, is topic of intense research. A constitutive law should provide a correct description of the spatio-temporal variability of parameters involved in the earthquake rupture process, which proves to be difficult. Widely applied empirical friction laws are derived from small-scale experiments (Brace and Byerlee, 1966; Ohnaka and Mogi, 1982; Ruina, 1983; Di Toro et al., 2005; Niemeijer et al., 2010) although the question of a proper scaling of the parameters to seismic faulting is evoked. Developed friction laws differ in correlating weakening of tractions on the fault surface to the slipped distance (slip-weakening law), the particle velocity on the fault (rate-dependent) and/or the history of the microstructural contacts (state-dependent). At high slip rates, non-linear physical weakening processes, as for example thermal pressurization of pore fluids, are thought to cause an observed extra-ordinary decrease of effective friction, referred to as fast-velocity weakening.

The implementation of slip-weakening friction has been presented in Pelties et al. (2012) and de la Puente et al. (2009). Here we advance to the following implementations of rate-and-state dependent constitutive relationships.

GMDD

6, 5981–6034, 2013

Verification of an ADER-DG method

C. Pelties et al.

Title Page

Abstract

Introduction

Conclusions

References

Tables

Figures

◀

▶

◀

▶

Back

Close

Full Screen / Esc

Printer-friendly Version

Interactive Discussion



7.1 Slow velocity weakening

Let the frictional strength of the fault evolve as follows:

$$\tau = \sigma \left(\mu_0 + a \ln \frac{V}{V_0} + b \ln \frac{V_0 \Theta}{L} \right), \quad (1)$$

where σ is the (constant) effective normal stress and μ_0 is the reference value of the friction coefficient at steady-state slip at reference sliding velocity V_0 . A rate-dependent part of the strength is proportional to the logarithm of the sliding velocity V and the frictional parameter a and is thought to reflect a thermally-activated Arrhenius process involving the breaking of atomic bonds at contact points bridging the sliding surface (Rice et al., 2001). A state-dependent part of the strength is proportional to the logarithm of the state variable Θ and the frictional parameter b , is thought to reflect the product of the true contact area and the intrinsic strength of those contacts. In the ageing law formulation the state variable evolves as

$$\dot{\Theta} = 1 - V \frac{\Theta}{L}, \quad (2)$$

whereas in the slip law formulation it is

$$\dot{\Theta} = -V \frac{\Theta}{L} \ln V \frac{\Theta}{L}. \quad (3)$$

The implementation of rate-and-state dependent friction into SeisSol follows roughly Kaneko et al. (2008). A 5 stage Newton–Raphson algorithm is used to determine the value of the slip rate in every sub time step obtained by the ADER integration scheme starting from the slip rate of the previous time step. The general implementation of frictional sliding into the ADER-DG algorithm is elaborated in Pelties et al. (2012). The state variable of the current time step is evaluated from the updated slip rate. Consecutively, the algorithm is repeated once.

Title Page

Abstract

Introduction

Conclusions

References

Tables

Figures

◀

▶

◀

▶

Back

Close

Full Screen / Esc

Printer-friendly Version

Interactive Discussion



In the form adopted in the following the frictional strength is determined by the slip velocity (V) and a state variable (Θ) as:

$$\tau = \sigma \left(a \operatorname{arcsinh} \left[\frac{V}{2V_0} \exp \frac{\Theta}{a} \right] \right), \quad (5)$$

where a is a positive coefficient quantifying a direct effect and V_0 is a reference slip rate. The state variable has units of slip and obeys the following evolution equation:

$$\dot{\Theta} = -\frac{V}{L} \left(\Theta - a \ln \left[\frac{2V_0}{V} \sinh \left\{ \frac{\mu_{ss}}{a} \right\} \right] \right), \quad (6)$$

where L is a characteristic slip scale. Following Noda et al. (2009) we regularize the steady-state friction coefficient μ_{ss} (obtained when $\dot{\Theta} = 0$) in the framework of rate-and-state friction in the slip law form:

$$\mu_{ss}(V) = \mu_s + \frac{\mu_0 - (b - a) \ln \left(\frac{V}{V_0} \right) - \mu_w}{\left[1 + \frac{V}{V_w} \right]^{1/8}}. \quad (7)$$

with μ_s being the static friction coefficient, μ_0 a reference friction coefficient, V_w a weakening velocity scale, μ_w the fully weakened friction coefficient and b a positive coefficient quantifying an evolution effect. In this formulation, the transition between low velocity friction and strongly velocity-weakened friction is relatively smooth, which is favorable for numerical accuracy (Dunham et al., 2011).

In Fig. 16 we show near-perfect agreement of ADER-DG with other high-order dynamic rupture software packages based on a variety of numerical methods: the multi-dimensional spectral boundary integral code MDSBI (Dunham, 2008), the three-dimensional spectral elements code SPECFEM3D (Kaneko et al., 2008) and the three-dimensional spectral boundary integral code SBIE (Lapusta and Liu, 2009). The agreement of the modeled dynamic rupture processes is depicted by the measured along-strike shear stress and slip rate on the fault outside the nucleation zone (Fig. 16a and c) and at the hypocenter (Fig. 16b and d).

Verification of an ADER-DG method

C. Pelties et al.

Title Page

Abstract

Introduction

Conclusions

References

Tables

Figures

◀

▶

◀

▶

Back

Close

Full Screen / Esc

Printer-friendly Version

Interactive Discussion



8 Conclusions

We showed the successful application of an ADER-DG scheme to advanced rupture dynamics test scenarios. We verified the performance by comparison to the established finite element method FaultMod in various faulting setups, including complex geometries and heterogeneity of physical model parameters across the fault. All shown time series of the ADER-DG method are raw and unfiltered. Due to the properties of the exact Riemann solver the solutions at the fault discontinuity remain free of spurious oscillations even under complex geometric and physical conditions.

We discussed some specific properties and outcomes of studying dynamic rupture with the ADER-DG method, as the resolution of small scale interface waves on a heterogeneously pre-stressed fault, the smoothness of results at a bi-material fault without experimentally motivated regularization, and the possible impact of a gap implementation in a fault branching system.

The method is specifically suited for dynamic rupture problems with complex fault geometry by allowing for mesh refinement and coarsening. This way, we can adapt the resolution to ensure fine sampling of the cohesive zone at the fault and save computational costs by increasing the mesh size where the dispersion properties of pure wave propagation allows. Propagation over distances of many wavelengths is enabled by a high-order accurate discretization of the wave equation. Furthermore, a smooth solution with minimized numerical artifacts of the frictional sliding is obtained to ensure physical reliability of the results.

We conclude that the advanced geometric flexibility combined with the enhanced accuracy makes it a competitive tool to study earthquake dynamics in complicated setups.

GMDD

6, 5981–6034, 2013

Verification of an ADER-DG method

C. Pelties et al.

Title Page

Abstract

Introduction

Conclusions

References

Tables

Figures

⏪

⏩

◀

▶

Back

Close

Full Screen / Esc

Printer-friendly Version

Interactive Discussion



Appendix A

Integration of fault dynamics across dissimilar material contacts into the ADER-DG algorithm

de la Puente et al. (2009) and Pelties et al. (2012) elaborated the full incorporation of fault dynamics in homogeneous materials into the ADER-DG framework. This approach, which is based on solving the inverse Riemann problem, differs substantially from the typically used traction-at-split-node (TSN) technique (Andrews, 1999; Day et al., 2005; Dalguer and Day, 2007). A Riemann problem is defined as an initial value problem based on a conservation law (here the hyperbolic partial differential equation) over a single discontinuity. Naturally, this problem occurs for Finite Volume (FV) and DG methods due to the discreteness of the grids. We solve this problem using the exact Riemann solver (or Godunov flux) which is a well known concept in numerical analysis to deliver a smooth solution (the Godunov state, which is indicated in the following by superscript G), although a discontinuous approximation of the physical unknowns is used. The most important benefits of this method compared to existing methods are the absence of spurious modes in the slip rate and the tetrahedral discretization enabling geometrical complexity of fault surfaces.

Here, we briefly review a general algorithm for implementing fault dynamics in schemes based on flux functions, neglecting the specifics of the ADER-DG method. This way, our implementation might be readily applied to a wide range of related numerical schemes. In particular, the algorithm is independent of the chosen time integration method. However, the impact of the implementation of fault dynamics on numerical properties as dispersion, diffusion and accuracy is expected to differ.

In general, we assume that the Coulomb failure criterion needs to be fulfilled at any point on the fault, e.g. at an integration point of the DG method:

$$|\tau^G| \leq \tau_S, \tag{A1}$$

Verification of an ADER-DG method

C. Pelties et al.

Title Page

Abstract

Introduction

Conclusions

References

Tables

Figures

◀

▶

◀

▶

Back

Close

Full Screen / Esc

Printer-friendly Version

Interactive Discussion



Verification of an ADER-DG method

C. Pelties et al.

Title Page

Abstract

Introduction

Conclusions

References

Tables

Figures

◀

▶

◀

▶

Back

Close

Full Screen / Esc

Printer-friendly Version

Interactive Discussion



with τ^G being the shear traction and τ_S the fault strength. We define the fault plane to be situated in the Cartesian y, z -plane and denote σ_i as the stress tensor, with $i = xx, yy, zz, xy, xz, yz$ as the normal and shear stresses, respectively. u, v, w are the particle velocities in x, y, z direction, respectively. An arbitrary fault side is defined as the + side, the opposing one as the --side. Corollary, $\Delta v = v^+ - v^-$ and $\Delta w = w^+ - w^-$ are the slip rates. Eq. (A1) prescribes that the shear traction $|\tau^G| = \sqrt{(\sigma_{xy}^G + \sigma_{xy}^0)^2 + (\sigma_{xz}^G + \sigma_{xz}^0)^2}$ is always lower or equal to the fault strength $\tau_S = \mu_f(\sigma_{xx}^G + \sigma_{xx}^0)$, where μ_f denotes the friction coefficient, which may be a function of slip, slip rate, state evolution variables and other frictional parameters. Variables denoted by superscript 0 are the corresponding initial values.

As long as the failure criterion is not fulfilled, the fault is locked and the physical stress and velocity variables, grouped into a vector \mathbf{Q} , are assigned to be the solution of the standard elastic wave propagation equations obtained from the Godunov state leading to $\mathbf{Q} = \mathbf{Q}^G$.

The set of equations to compute the Godunov states accounting for a material contrast across the fault, based on Toro (1999), LeVeque (2002), de la Puente et al. (2009) and Pelties et al. (2012), is given by:

$$\sigma_{xx}^G = \sigma_{xx}^+ + \frac{[(\sigma_{xx}^- - \sigma_{xx}^+) + c_p^- \rho^- (u^- - u^+)] c_p^+ \rho^+}{c_p^+ \rho^+ + c_p^- \rho^-}$$

$$\sigma_{xy}^G = \sigma_{xy}^+ + \frac{[(\sigma_{xy}^- - \sigma_{xy}^+) + c_s^- \rho^- (v^- - v^+)] c_s^+ \rho^+}{c_s^+ \rho^+ + c_s^- \rho^-}$$

$$\sigma_{xz}^G = \sigma_{xz}^+ + \frac{[(\sigma_{xz}^- - \sigma_{xz}^+) + c_s^- \rho^- (w^- - w^+)] c_s^+ \rho^+}{c_s^+ \rho^+ + c_s^- \rho^-}$$

$$u^G = u^+ + \frac{\sigma_{xx}^G - \sigma_{xx}^+}{c_p^+ \rho^+}$$

$$v^G = v^+ + \frac{\sigma_{xy}^G - \sigma_{xy}^+}{c_s^+ \rho^+} \quad (\text{A2})$$

$$w^G = w^+ + \frac{\sigma_{xz}^G - \sigma_{xz}^+}{c_s^+ \rho^+},$$

where ρ denotes density, c_p P wave velocity and c_s S wave velocity. Note that σ_{yy}, σ_{zz} and σ_{yz} are associated to zero wave speeds and do not contribute to the solution of the Riemann problem. Thus, we do not compute them.

In case $|\tau^G| = \tau_S$ the fault fails and slip is declared. Then, we impose the shear stresses to be

$$\sigma_{xy} = \frac{\sigma_{xy}^G + \sigma_{xy}^0}{|\tau^G|} \tau_S \quad (\text{A3})$$

$$\sigma_{xz} = \frac{\sigma_{xz}^G + \sigma_{xz}^0}{|\tau^G|} \tau_S$$

and use Eq. (A3) to obtain the slip rates

$$\Delta v = \left(\frac{1}{c_s^+ \rho^+} + \frac{1}{c_s^- \rho^-} \right) (\sigma_{xy} - \sigma_{xy}^G) \quad (\text{A4})$$

$$\Delta w = \left(\frac{1}{c_s^+ \rho^+} + \frac{1}{c_s^- \rho^-} \right) (\sigma_{xz} - \sigma_{xz}^G),$$

Verification of an ADER-DG method

C. Pelties et al.

Title Page

Abstract

Introduction

Conclusions

References

Tables

Figures

◀

▶

◀

▶

Back

Close

Full Screen / Esc

Printer-friendly Version

Interactive Discussion



Verification of an ADER-DG method

C. Pelties et al.

Title Page

Abstract

Introduction

Conclusions

References

Tables

Figures

◀

▶

◀

▶

Back

Close

Full Screen / Esc

Printer-friendly Version

Interactive Discussion



In the case of on-going slip, we impose v and w individually for the + and – side as

$$v^+ = v^+ + \frac{\sigma_{xy} - \sigma_{xy}^+}{c_s^+ \rho^+}$$

$$v^- = v^- + \frac{\sigma_{xy} - \sigma_{xy}^-}{c_s^- \rho^-}$$

$$w^+ = w^+ + \frac{\sigma_{xz} - \sigma_{xz}^+}{c_s^+ \rho^+}$$

$$w^- = w^- + \frac{\sigma_{xz} - \sigma_{xz}^-}{c_s^- \rho^-}.$$

(A5)

In summary, this implementation allows for modeling fault dynamics in dissimilar materials across the fault featuring identical numerical properties to the purely homogeneous case. For identical material properties at the + and – sides of the fault the above equations collapse to the system presented in Pelties et al. (2012).

Appendix B

Influence of Prakash–Clifton regularization

As remarked in the introduction of Sect. 6, ill-posed bi-material problems need to be regularized to ensure convergence. Regularization can be achieved by Prakash–Clifton regularization as introduced by Prakash and Clifton (1993) and Cochard and Rice (2000), which is an experimental based law relating the shear strength evolution continuously to abrupt changes of normal stress. We implemented optional Prakash–Clifton regularization (not used for the benchmark presented in Sect. 6) in the simplified form:

$$\dot{\tau}^S = -\frac{|V| + V^*}{L} \left(\tau^S - \mu \max(0, -\sigma_n) \right), \quad (\text{B1})$$

where τ^S is the frictional strength, V is the slip velocity, V^* the characteristic slip-velocity, L the characteristic distance, μ the friction coefficient, and σ_n the normal stress.

Evidently, the amount of added damping or regularization could potentially have a significant influence on the result, as was elaborated by Cochard and Rice (2000). Therefore, we present here the influence of the regularization on the ADER-DG algorithm to provide guidance for users on the impact of regularization. To this end, we summarize in the following our findings from the ill-posed TPV7 test case scenario.

The setup is identical to TPV6 except that the far side features a wave speed reduction of 20% at same material density for both sides of the fault. We applied a resolution of $h = 200$ m and $\mathcal{O}4$ in space and time.

While V^* was set to 1 ms^{-1} in our setup, we varied the characteristic distance L . Figure 17 presents results with choosing $L = 0.2, 0.05, 0.01$ and without regularization for comparison. As expected, the values of $L = 0.2, 0.05$ lead to large discrepancies in the peak slip rate as well as in the rupture arrival time. However, even a small characteristic distance of $L = 0.01$ produces a visible difference in the time series of shear stress and slip rate.

As we reduce L we find convergence towards the solution without Prakash–Clifton regularization, instead of the noisy solution expected for the ill-posed problem solved with a high resolution (small element size h and high order of accuracy \mathcal{O}) (Cochard and Rice, 2000). We conclude that there is an additional source of regularization in our simulations: the intrinsic numerical dissipation of ADER-DG with Godunov fluxes (see Sect. 2). This is not necessarily trivial: other forms of numerical dissipation may not be strong enough to regularize the problem by counteracting the growth of the unstable short-wavelength modes. Our simulations then contain two efficient regularization mechanisms: (1) Prakash–Clifton regularization and (2) ADER-DG’s numerical dissipation. The characteristic time scale of the Prakash–Clifton regularization is

Verification of an ADER-DG method

C. Pelties et al.

Title Page	
Abstract	Introduction
Conclusions	References
Tables	Figures
◀	▶
◀	▶
Back	Close
Full Screen / Esc	
Printer-friendly Version	
Interactive Discussion	



**Verification of an
ADER-DG method**

 C. Pelties et al.

[Title Page](#)
[Abstract](#)
[Introduction](#)
[Conclusions](#)
[References](#)
[Tables](#)
[Figures](#)
[◀](#)
[▶](#)
[◀](#)
[▶](#)
[Back](#)
[Close](#)
[Full Screen / Esc](#)
[Printer-friendly Version](#)
[Interactive Discussion](#)


edited by: Abercrombie, R., McGarr, A., Di Toro, G., and Kanamori, H., Wiley Online Library, 255–261, doi:10.1029/170GM25, 2006. 5988

Andrews, D. J.: Test of two methods for faulting in finite-difference calculations, *Bull. Seism. Soc. Am.*, 89, 931–937, 1999. 5985, 5986, 6000

5 Andrews, D. J.: Rupture dynamics with energy loss outside the slip zone, *J. Geophys. Res.*, 110, B01307, doi:10.1029/2004JB003191, 2005. 5983

Andrews, D. J., Hanks, T. C., Whitney, J. W.: Physical limits on ground motion at Yucca Mountain, *Bull. Seism. Soc. Am.*, 97, 1771–1792, 2007. 5988

10 Aochi, H., Madariaga, R., and Fukuyama, E.: Constraint of fault parameters inferred from non-planar fault modeling, *Geochem. Geophys. Geosys.*, 4, 1020, doi:10.1029/2001GC000207, 2003. 5984

Barall, M.: A grid-doubling finite-element technique for calculating dynamic three-dimensional spontaneous rupture on an earthquake fault, *Geophys. J. Int.*, 178, 845–859, doi:10.1111/j.1365-246X.2009.04190.x, 2009. 5986, 5987

15 Barbot, S., Lapusta, N., and Avouac, J.: Under the hood of the earthquake machine: toward predictive modeling of the seismic cycle, *Science*, 336, 707–710, doi:10.1126/science.1218796, 2012. 5982

Bhat, H. S., Olives, M., Dmowska, R., and Rice, J. R.: Role of fault branches in earthquake rupture dynamics, *J. Geophys. Res.-S. Ea.*, 112, 2156–2202, doi:10.1029/2007JB005027, 2007. 5982

20 Boatwright, J. and Quin, H.: The seismic radiation from a 3-D dynamic model of a complex rupture process; Part I, Confined ruptures, in: *Earthquake Source Mechanics*, Geophysical Monograph, edited by: Das, S., Boatwright, J., and Scholz, C. H., 37, 97–109, 1986. 5988

Brace, W. and Byerlee, J.: Stick-slip as a mechanism for earthquakes, *Science*, 153, 990–992, doi:10.1126/science.153.3739.990, 1966. 5995

25 Brietzke, G., Cochard, A., and Igel, H.: Importance of bimaterial interfaces for earthquake dynamics and strong ground motion, *Geophys. J. Int.*, 178, 921–938, doi:10.1111/j.1365-246X.2009.04209.x, 2009. 5984, 5993

Cochard, A. and Madariaga, R.: Dynamic faulting under rate-dependent friction, *Pure Appl. Geophys.*, 142, 419–445, 1994. 5984

30 Cochard, A. and Rice, J.: Fault rupture between dissimilar materials: ill-posedness, regularization, and slip-pulse response, *J. Geophys. Res.*, 105, 25891–25907, doi:10.1029/2000JB900230, 2000. 6003, 6004

**Verification of an
ADER-DG method**

 C. Pelties et al.

[Title Page](#)
[Abstract](#)
[Introduction](#)
[Conclusions](#)
[References](#)
[Tables](#)
[Figures](#)
[◀](#)
[▶](#)
[◀](#)
[▶](#)
[Back](#)
[Close](#)
[Full Screen / Esc](#)
[Printer-friendly Version](#)
[Interactive Discussion](#)


- Cui, Y., Olsen, K., Jordan, T., Lee, K., Zhou, J., Small, P., Roten, D., Ely, G., Panda, D., Chourasia, A., Levesque, J., Day, S., and Maechling, P.: Scalable earthquake simulation on petascale supercomputers, in: International Conference for High Performance Computing, Networking, Storage and Analysis (SC), 1–20, doi:10.1109/SC.2010.45, 2010. 5982
- 5 Dalguer, L. and Day, S.: Staggered-grid split-node method for spontaneous rupture simulation, *J. Geophys. Res.*, 112, B02302, doi:10.1029/2006JB004467, 2007. 5983, 5985, 5986, 6000
- Dalguer, L., Irikura, K., Riera, J., and Chiu, H.: The importance of the dynamic source effects on strong ground motion during the 1999 Chi-Chi, Taiwan, earthquake: brief interpretation of the damage distribution on buildings, *Bull. Seism. Soc. Am.*, 91, 1112–1127, 2001. 5988
- 10 Daub, E., Manning, M., and Carlson, J.: Pulse-like, crack-like, and supershear earthquake ruptures with shear strain localization, *J. Geophys. Res.*, 115, B05311, doi:10.1029/2009JB006388, 2010. 5982
- Day, S. M.: Three-dimensional finite-difference simulation of fault dynamics: rectangular faults with fixed rupture velocity, *Bull. Seism. Soc. Am.*, 72, 705–727, 1982. 5988
- 15 Day, S. M., Yu, G., and Wald, D. J.: Dynamic stress changes during earthquake rupture, *Bull. Seism. Soc. Am.*, 88, 512–522, 1998. 5984
- Day, S. M., Dalguer, L. A., Lapusta, N., and Liu, Y.: Comparison of finite difference and boundary integral solutions to three-dimensional spontaneous rupture, *J. Geophys. Res.*, 110, B12307, doi:10.1029/2005JB003813, 2005. 5983, 5985, 5986, 6000
- 20 DeDontney, N., Rice, J., and Dmowska, R.: Influence of material contrast on fault branching behavior, *Geophys. Res. Lett.*, 38, L14305, doi:10.1029/2011GL047849, 2011. 5982, 5991, 5993
- de la Puente, J., Ampuero, J.-P., and Käser, M.: Dynamic rupture modeling on unstructured meshes using a discontinuous Galerkin method, *J. Geophys. Res.*, 114, B10302, doi:10.1029/2008JB006271, 2009. 5984, 5985, 5995, 6000, 6001
- Di Toro, G., Nielsen, S., and Pennacchioni, G.: Earthquake rupture dynamics frozen in exhumed ancient faults, *Nature*, 436, 1009–1012, doi:10.1038/nature03910, 2005. 5983, 5995
- Di Toro, G., Han, R., Hirose, T., De Paola, N., Nielsen, S., Mizoguchi, K., Ferri, F., Cocco, M., and Shimamoto, T.: Fault lubrication during earthquakes, *Nature*, 471, 494–498, doi:10.1038/nature09838, 2011. 5997
- 30 Dieterich, J. H.: Time-dependent friction and the mechanics of stick-slip, *Pure Appl. Geophys.*, 116, 790–806, doi:10.1007/BF00876539, 1978. 5983

**Verification of an
ADER-DG method**

 C. Pelties et al.

[Title Page](#)
[Abstract](#)
[Introduction](#)
[Conclusions](#)
[References](#)
[Tables](#)
[Figures](#)
[◀](#)
[▶](#)
[◀](#)
[▶](#)
[Back](#)
[Close](#)
[Full Screen / Esc](#)
[Printer-friendly Version](#)
[Interactive Discussion](#)


- Duan, B. and Day, S.: Inelastic strain distribution and seismic radiation from rupture of a fault kink, *J. Geophys. Res.-S. Ea.*, 113, 2156–2202, doi:10.1029/2008JB005847, 2008. 5983
- Dumbser, M. and Käser, M.: An arbitrary high order discontinuous Galerkin method for elastic waves on unstructured meshes II: The three-dimensional case, *Geophys. J. Int.*, 167, 319–336, 2006. 5984, 5985
- 5 Dunham, E.: Dissipative interface waves and the transient response of a three-dimensional sliding interface with Coulomb friction, *J. Mech. Phys. Sol.*, 53, 327–357, doi:10.1016/j.jmps.2004.07.003, 2005. 5990
- Dunham, E.: Conditions governing the occurrence of supershear ruptures under slip-weakening friction, *J. Geophys. Res.*, 112, 1–24, 2007. 5982, 5988
- 10 Dunham, E. M.: MDSBI: Multi-Dimensional Spectral Boundary Integral Code, version 4.1.7, available at: <http://pangea.stanford.edu/~edunham/codes/codes.html>, 2008. 5998, 6033
- Dunham, E. M., Belanger, D., Cong, L., and Kozdon, J. E.: Earthquake ruptures with strongly rate-weakening friction and off-fault plasticity, Part 1: planar faults, *Bull. Seism. Soc. Am.*, 101, 2296–2307, 2011. 5997, 5998
- 15 Ely, G. P., Day, S. M., and Minster, J.-B.: Dynamic rupture models for the southern San Andreas Fault, *Bull. Seis. Soc. Am.*, 100, 131–150, doi:10.1785/0120090187, 2010. 5982
- Gabriel, A.-A., Ampuero, J.-P., Dalguer, L. A., and Mai, P. M.: The transition of dynamic rupture modes in elastic media under velocity-weakening friction, *J. Geophys. Res.*, 117, 0148–0227, doi:10.1029/2012JB009468, 2012. 5982
- 20 Gabriel, A.-A., Ampuero, J.-P., Dalguer, L. A., and Mai, P. M.: Source properties of dynamic rupture pulses with off-fault plasticity, *J. Geophys. Res.*, 118, 4117–4126, doi:10.1002/jgrb.50213, 2013. 5982, 5997
- Harris, R. A. and Day, S. M.: Effects of a low-velocity zone on a dynamic rupture, *Bull. Seism. Soc. Am.*, 87, 1267–1280, 1997. 5993
- 25 Harris, R. A., Barall, M., Archuleta, R., Dunham, E., Aagaard, B., Ampuero, J.-P., Bhat, H., Cruz-Atienza, V., Dalguer, L., Dawson, P., Day, S., Duan, B., Ely, G., Kaneko, Y., Kase, Y., Lapusta, N., Liu, Y., Ma, S., Oglesby, D., Olsen, K., Pitarka, A., Song, S., and Templeton, E.: The SCEC/USGS dynamic earthquake rupture code verification exercise, *Seismol. Res. Lett.*, 80, 119–126, doi:10.1785/gssrl.80.1.119, 2009. 5984
- 30 Harris, R., Barall, M., Andrews, D., Duan, B., Ma, S., Dunham, E., Gabriel, A., Kaneko, Y., Kase, Y., Aagaard, B., Oglesby, D., Ampuero, J., Hanks, T., and Abrahamson, N.: Verifying

**Verification of an
ADER-DG method**

C. Pelties et al.

[Title Page](#)
[Abstract](#)
[Introduction](#)
[Conclusions](#)
[References](#)
[Tables](#)
[Figures](#)
[◀](#)
[▶](#)
[◀](#)
[▶](#)
[Back](#)
[Close](#)
[Full Screen / Esc](#)
[Printer-friendly Version](#)
[Interactive Discussion](#)


- a computational method for predicting extreme ground motion, *Seismol. Res. Lett.*, 82, 638–644, doi:10.1785/gssrl.82.5.638, 2011. 5982, 5984
- Huang, Y., and Ampuero, J.-P.: Pulse-like ruptures induced by low-velocity fault zones, *J. Geophys. Res.*, 116, B12307, doi:10.1029/2011JB008684, 2011. 5982
- 5 Huang, Y., Ampuero, J.-P., and Kanamori, H.: Slip-weakening models of the 2011 Tohoku-Oki earthquake and constraints on stress drop and fracture energy, *Pure Appl. Geophys.*, ISSN 14209136, 1–14, 2013. 5987
- Hughes, T.: *The finite element method: linear static and dynamic finite element analysis*, Dover Civil and Mechanical Engineering Series, Dover Publications, 2000. 5986
- 10 Kaneko, Y., Lapusta, N., and J.-P. Ampuero: Spectral element modeling of spontaneous earthquake rupture on rate and state faults: effect of velocity-strengthening friction at shallow depths, *J. Geophys. Res.*, 113, B09317, doi:10.1029/2007JB005553, 2008. 5984, 5996, 5998, 6033
- Karypis, G. and Kumar, V.: Multilevel k-way partitioning scheme for irregular graphs, *J. Parallel Distrib. Comput.*, 48, 96–129, 1998. 5985
- 15 Käser, M. and Dumbser, M.: An arbitrary high order discontinuous Galerkin method for elastic waves on unstructured meshes I: the two-dimensional isotropic case with external source terms, *Geophys. J. Int.*, 166, 855–877, 2006. 5984, 5985
- Käser, M., Hermann, V., and de la Puente, J.: Quantitative accuracy analysis of the discontinuous galerkin method for seismic wave propagation, *Geophys. J. Int.*, 173, 990–999, 2008. 5989
- 20 Lapusta, N. and Liu, Y.: Three-dimensional boundary integral modeling of spontaneous earthquake sequences and aseismic slip, *J. Geophys. Res.*, 114, B09303, doi:10.1029/2008JB005934, 2009. 5998, 6033
- 25 LeVeque, R.: *Finite Volume Methods for Hyperbolic Problems*, Cambridge University Press, Cambridge, 2002. 5985, 6001
- Ma, S. and Andrews, D. J.: Inelastic off-fault response and three-dimensional dynamics of earthquake rupture on a strike-slip fault, *J. Geophys. Res.*, 115, B04304, doi:10.1029/2009JB006382, 2010. 5982
- 30 Ma, S. and Archuleta, R. J.: Radiated seismic energy based on dynamic rupture models of faulting, *J. Geophys. Res.*, 111, B05315, doi:10.1029/2005JB004055, 2006. 5988
- Ma, S. and Beroza, G. C.: Rupture dynamics on a bimaterial interface for dipping faults, *Bull. Seism. Soc. Am.*, 98, 1642–1658, doi:10.1785/0120070201, 2008. 5988

**Verification of an
ADER-DG method**

 C. Pelties et al.

[Title Page](#)
[Abstract](#)
[Introduction](#)
[Conclusions](#)
[References](#)
[Tables](#)
[Figures](#)
[◀](#)
[▶](#)
[◀](#)
[▶](#)
[Back](#)
[Close](#)
[Full Screen / Esc](#)
[Printer-friendly Version](#)
[Interactive Discussion](#)


- Madariaga, R.: Radiation from a finite reverse fault in a half space, *Pure Appl. Geophys.*, 160, 555–577, doi:10.1007/PL00012550, 2003. 5987
- Niemeijer, A., Marone, C., and Elsworth, D.: Frictional strength and strain weakening in simulated fault gouge: competition between geometrical weakening and chemical strengthening, *J. Geophys. Res.*, 115, B10207, doi:10.1029/2009JB000838, 2010. 5995
- 5 Noda, H., Dunham, E. M., and Rice, J. R.: Earthquake ruptures with thermal weakening and the operation of major faults at low overall stress levels, *J. Geophys. Res.*, 114, B07302, doi:10.1029/2008JB006143, 2009. 5998
- Oglesby, D. D. and Day, S. M.: Stochastic fault stress: Implications for fault dynamics and ground motion, *Bull. Seism. Soc. Am.*, 92, 3006–3021, 2002. 5988
- 10 Oglesby, D. D., Archuleta, R. J., and Nielsen, S. B.: Earthquakes on dipping faults: the effects of broken symmetry, *Science*, 280, 1055–1059, doi:10.1126/science.280.5366.1055, 1998. 5987
- Oglesby, D. D., Day, S. M., Li, Y.-G., and Vidale, J. E.: The 1999 Hector Mine earthquake: the dynamics of a branched fault system, *Bull. Seism. Soc. Am.*, 93, 2459–2476, doi:10.1785/0120030026, 2003. 5982
- 15 Ohnaka, M. and Mogi, K.: Frequency characteristics of acoustic emission in rocks under uniaxial compression and its relation to the fracturing process to failure, *J. Geophys. Res.*, 87, 3873–3884, doi:10.1029/JB087iB05p03873, 1982. 5983, 5995
- 20 Pacheco, J. F. and Sykes, L. R.: Seismic moment catalog of large shallow earthquakes, 1900 to 1989, *Bull. Seism. Soc. Am.*, 82, 1306–1349, 1992. 5986
- Pelties, C., Käser, M., Hermann, V., and Castro, C.: Regular vs. irregular meshing for complicated models and their effect on synthetic seismograms, *Geophys. J. Int.*, 183, 1031–1051, doi:10.1111/j.1365-246X.2010.04777.x, 2010. 5989
- 25 Pelties, C., de la Punte, P., Ampuero, J.-P., Brietzke, G. B., and Käser, M.: Three-dimensional dynamic rupture simulation with a high-order discontinuous Galerkin method on unstructured tetrahedral meshes, *J. Geophys. Res.*, 117, B02309, doi:10.1029/2011JB008857, 2012. 5984, 5985, 5986, 5995, 5996, 6000, 6001, 6003
- Prakash, V. and Clifton, R. J.: Time resolved dynamic friction measurements in pressure shear, *Experimental Techniques in the Dynamics of Deformable Solids*, 165, 33–48, 1993. 6003
- 30 Rice, J. R.: Heating and weakening of faults during earthquake slip, *J. Geophys. Res.*, 111, B05311, doi:10.1029/2005JB004006, 2006. 5997

**Verification of an
ADER-DG method**

 C. Pelties et al.

[Title Page](#)
[Abstract](#)
[Introduction](#)
[Conclusions](#)
[References](#)
[Tables](#)
[Figures](#)
[◀](#)
[▶](#)
[◀](#)
[▶](#)
[Back](#)
[Close](#)
[Full Screen / Esc](#)
[Printer-friendly Version](#)
[Interactive Discussion](#)


Rice, J. R., Lapusta, N., and Ranjith, K.: Rate and state dependent friction and the stability of sliding between elastically deformable solids, *J. Mech. Phys. Solids*, 49, 1865–1898, 2001. 5996

Roten, D., Olsen, K. B., Pechmann, J. C., Cruz-Atienza, V. M., and Magistrale, H.: 3-D simulations of M 7 earthquakes on the Wasatch Fault, Utah, Part I: Long-period (0–1 Hz) ground motion, *Bull. Seis. Soc. Am.*, 101, 2045–2063, doi:10.1785/0120110031, 2011. 5982

Rudnicki, J. and Wu, M.: Mechanics of dip-slip faulting in an elastic half-space, *J. Geophys. Res.*, 100, 22122–22173, 1995. 5988

Ruina, A.: Slip instability and state variable friction laws, *J. Geophys. Res.*, 88, 10359–10370, doi:10.1029/JB088iB12p10359, 1983. 5995

Schwartz, D. P., Haeussler, P. J., Seitz, G. G., and Dawson, T. E.: Why the 2002 Denali fault rupture propagated onto the Totschunda fault: implications for fault branching and seismic hazards, *J. Geophys. Res.*, 117, B11304, doi:10.1029/2011JB008918, 2012. 5990

Templeton, E. L. and Rice, J. R.: Off-fault plasticity and earthquake rupture dynamics: 1. Dry materials or neglect of fluid pressure changes, *J. Geophys. Res.*, 113, B09306, doi:10.1029/2007JB005529, 2008. 5982

Thurber, C., Zhang, H., Waldhauser, F., Hardebeck, J., Michael, A., and Eberhart-Phillips, D.: Three-dimensional compressional wavespeed model, earthquake relocations, and focal mechanisms for the Parkfield, California, Region, *B. Seismol. Soc. Am.*, 96, S38–S49, doi:10.1785/0120050825, 2006. 5993

Toro, E.: *Riemann Solvers and Numerical Methods for Fluid Dynamics*, Springer, 2nd Edn., 1999. 5985, 6001

Zhou, J., Cui, Y., Poyraz, E., Choi, D. J., and Guest, C. C.: Multi-GPU implementation of a 3-D finite difference time domain earthquake code on heterogeneous supercomputers, in: *Proceedings of the International Conference on Computational Science (ICCS)*, Barcelona, Spain, 5–7 June 2013, 1255–1264, doi:10.1016/j.procs.2013.05.292, 2013. 5982

Verification of an ADER-DG method

C. Pelties et al.

Title Page

Abstract

Introduction

Conclusions

References

Tables

Figures

◀

▶

◀

▶

Back

Close

Full Screen / Esc

Printer-friendly Version

Interactive Discussion



Table 2. SCEC Test Case 17 simulation parameters.

c_P	P wave speed	6000 ms^{-1}
c_S	Shear wave speed	3464 ms^{-1}
ρ	Density	2670 kg m^{-3}
A_{fault}	Faulting area	$48.0 \text{ km} \times 19.5 \text{ km}$
h	Element size	200 m
\mathcal{O}	Spatio-temporal order of accuracy	4

Verification of an
ADER-DG method

C. Pelties et al.

Title Page

Abstract

Introduction

Conclusions

References

Tables

Figures

◀

▶

◀

▶

Back

Close

Full Screen / Esc

Printer-friendly Version

Interactive Discussion

**Table 3.** SCEC Test Case 15 simulation parameters.

c_P	P wave speed	6000 ms^{-1}
c_S	Shear wave speed	3464 ms^{-1}
ρ	Density	2670 kg m^{-3}
μ_s	Static friction coefficient	0.677
μ_d	Dynamic friction coefficient	0.525
D_c	Slip-weakening critical distance	0.4 m
σ_0	Background normal stress	120.0 MPa
τ_0^{main}	Background shear stress on main fault	−70.0 MPa
τ_0^{branch}	Background shear stress on branch fault	−78.0 MPa
τ_0^{nuc}	Nucleation shear stress along-dip	−81.6 MPa
A_{nuc}	Nucleation size	3 km × 3 km
$A_{\text{fault}}^{\text{main}}$	Faulting area	28 km × 15 km
$A_{\text{fault}}^{\text{branch}}$	Faulting area	12 km × 15 km
h	Element size	300 m
\mathcal{O}	Spatio-temporal order of accuracy	4

Verification of an
ADER-DG method

C. Pelties et al.

Title Page

Abstract

Introduction

Conclusions

References

Tables

Figures

◀

▶

◀

▶

Back

Close

Full Screen / Esc

Printer-friendly Version

Interactive Discussion

**Table 4.** SCEC Test Case 6 simulation parameters.

ρ_{near}	Density	2670 kg m^{-3}
$c_{\text{P,near}}$	P wave speed	6000 ms^{-1}
$c_{\text{S,near}}$	Shear wave speed	3464 ms^{-1}
ρ_{far}	Density	2225 kg m^{-3}
$c_{\text{P,far}}$	P wave speed	3750 ms^{-1}
$c_{\text{S,far}}$	Shear wave speed	2165 ms^{-1}
μ_{s}	Static friction coefficient	0.677
μ_{d}	Dynamic friction coefficient	0.525
D_{c}	Slip-weakening critical distance	0.4 m
σ_0	Background normal stress	120.0 MPa
τ_0	Background shear stress on main fault	70.0 MPa
τ_0^{nuc}	Nucleation shear stress along-dip	81.6 MPa
A_{nuc}	Nucleation size	3 km \times 3 km
A_{fault}	Faulting area	30 km \times 15 km
h	Element size	200 m
\mathcal{O}	Spatio-temporal order of accuracy	4

Verification of an
ADER-DG method

C. Pelties et al.

Title Page

Abstract

Introduction

Conclusions

References

Tables

Figures

◀

▶

◀

▶

Back

Close

Full Screen / Esc

Printer-friendly Version

Interactive Discussion

**Table 5.** SCEC Test Case TPV101 simulation parameters.

c_P	P wave speed	6000 m s^{-1}
c_S	Shear wave speed	3464 m s^{-1}
ρ	Density	2670 kg m^{-3}
μ_0	Reference friction coefficient TPV10	0.6
V_0	Reference slip velocity	10^{-6} m s^{-1}
$a(x, y)$	Frictional evolution coefficient	$0.008 + \Delta a(x, y)$
b	Frictional state coefficient	0.012
L	characteristic slip scale	0.02 m
V_{ini}	Initial sliding velocity	$10^{-12} \text{ m s}^{-1}$
Θ_{ini}	Initial state variable	$1.60624 \times 10^9 \text{ s} + \Delta\Theta(x, y)$
τ_0	Background shear stress along-strike	75 MPa
σ_0	Background normal stress	120 MPa
$\Delta\tau_0$	Nucleating background shear stress perturbation	25 MPa
A_{nuc}	Nucleation radius	3 km
A_{nuc}	Nucleation time	1 s
(x_0, y_0)	Hypocenter	(0, 7.5 km)
A_{fault}	Velocity-weakening faulting area	30 km \times 15 km
h	Element size	250 m
O	Spatio-temporal order of accuracy	4

Verification of an
ADER-DG method

C. Pelties et al.

Table 6. SCEC Test Case TPV103 simulation parameters which differ from Test Case TPV101.

$a(x, y)$	Frictional evolution coefficient	$0.01 + \Delta a(x, y)$
b	Frictional state coefficient	0.014
L	characteristic slip scale distance	0.4 m
V_w	weakening sliding velocity	$0.1 + \Delta V_w(x, y) \text{ m s}^{-1}$
μ_w	weakening friction coefficient	0.2
V_{ini}	Initial sliding velocity	$10^{-16} \text{ m s}^{-1}$
Θ_{ini}	Initial state variable	$0.5636 \text{ s} + \Delta \Theta(x, y)$
τ_0	Background shear stress along-strike	40 MPa
$\Delta \tau_0$	Nucleating background shear stress perturbation	45 MPa
A_{fault}	Velocity-weakening faulting area	30 km \times 15 km
h	Element size	250 m
O	Spatio-temporal order of accuracy	4

Title Page

Abstract

Introduction

Conclusions

References

Tables

Figures

◀

▶

◀

▶

Back

Close

Full Screen / Esc

Printer-friendly Version

Interactive Discussion



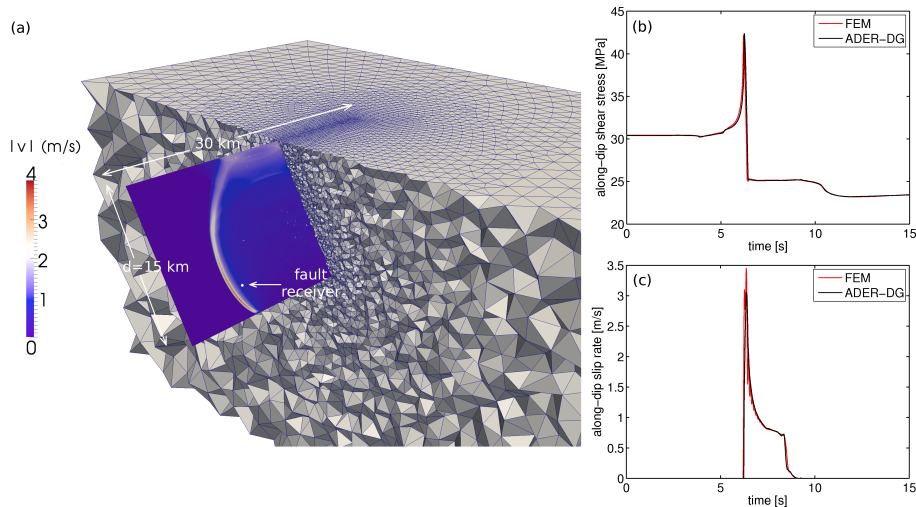


Fig. 1. (a) Asymmetric unstructured mesh discretizing the dipping fault setup of benchmark problems TPV10 and TPV11, and slip rate on the fault plane at $t = 7.4$ s of TPV10 (subshear scenario). (b) Along-dip slip rate and (c) along-dip shear stress of an on-fault receiver at 7.5 km along-strike and 12 km along-dip of TPV10. The ADER-DG solution is shown in black, the FEM comparison solution in red.

Verification of an ADER-DG method

C. Pelties et al.

Title Page

Abstract

Introduction

Conclusions

References

Tables

Figures

◀

▶

◀

▶

Back

Close

Full Screen / Esc

Printer-friendly Version

Interactive Discussion



Verification of an ADER-DG method

C. Pelties et al.

Title Page

Abstract

Introduction

Conclusions

References

Tables

Figures

◀

▶

◀

▶

Back

Close

Full Screen / Esc

Printer-friendly Version

Interactive Discussion

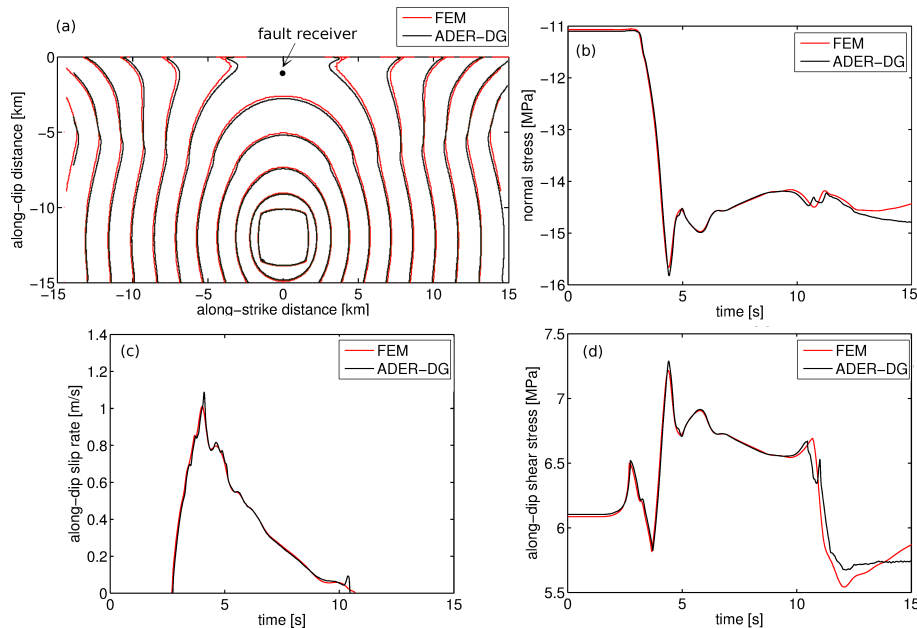


Fig. 2. Supershear and free surface effects in TPV11. **(a)** Rupture front contours on the fault plane every 0.5 s. **(b)** Normal stress, **(c)** along-dip slip rate and **(d)** along-dip shear stress at an on-fault receiver located 0 km along-strike and 1.5 km along-dip. The ADER-DG solution is shown in black, the FEM comparison solution in red.

Verification of an
ADER-DG method

C. Pelties et al.

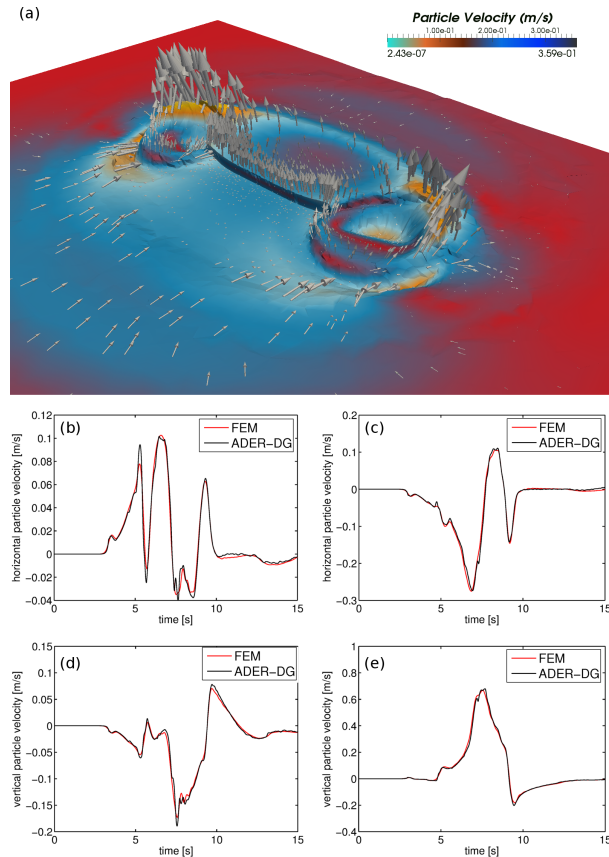


Fig. 3. (a) Asymmetric ground motion (absolute particle velocity) in the surrounding of the dipping fault at $t \approx 8$ s in TPV10. (b) and (c) are horizontal ground velocity time series at seismic stations located 3 km away from the fault trace and 12 km along-strike on the foot wall and hanging wall, respectively. (d) and (e) are the vertical ground velocities at the same stations. The ADER-DG solution is shown in black, the FEM comparison solution in red.

Title Page

Abstract

Introduction

Conclusions

References

Tables

Figures

◀

▶

◀

▶

Back

Close

Full Screen / Esc

Printer-friendly Version

Interactive Discussion



Verification of an
ADER-DG method

C. Pelties et al.

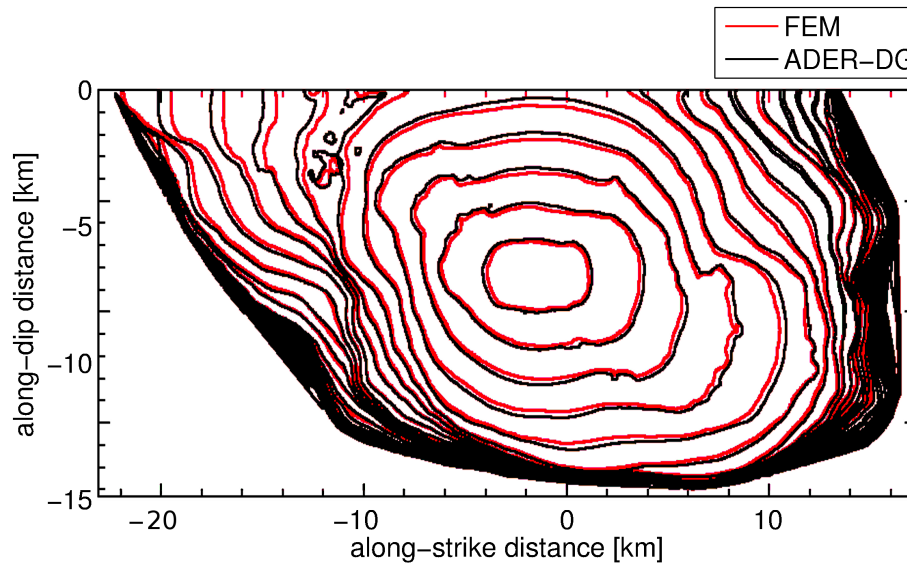


Fig. 4. Rupture front every 0.5 s of problem TPV17 with heterogeneous initial stress conditions. The ADER-DG rupture front is indicated in black, the FEM comparison solution in red.

[Title Page](#)[Abstract](#)[Introduction](#)[Conclusions](#)[References](#)[Tables](#)[Figures](#)[◀](#)[▶](#)[◀](#)[▶](#)[Back](#)[Close](#)[Full Screen / Esc](#)[Printer-friendly Version](#)[Interactive Discussion](#)

Verification of an
ADER-DG method

C. Pelties et al.

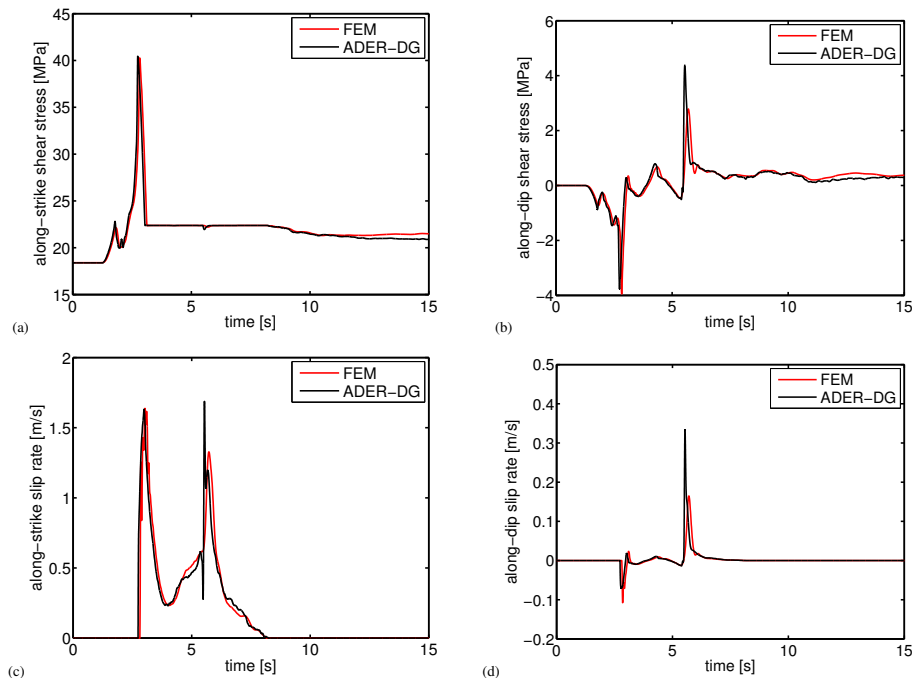


Fig. 5. Shear stresses and slip rates for TPV17 at a receiver located 9 km deep and -9 km along strike. A sharp feature caused by the interface wave can be identified in the along-strike slip rate (c) at $t \sim 5.5$ s. The ADER-DG solution is shown in black, the FEM comparison solution in red.

[Title Page](#)[Abstract](#)[Introduction](#)[Conclusions](#)[References](#)[Tables](#)[Figures](#)[◀](#)[▶](#)[◀](#)[▶](#)[Back](#)[Close](#)[Full Screen / Esc](#)[Printer-friendly Version](#)[Interactive Discussion](#)

Verification of an ADER-DG method

C. Pelties et al.

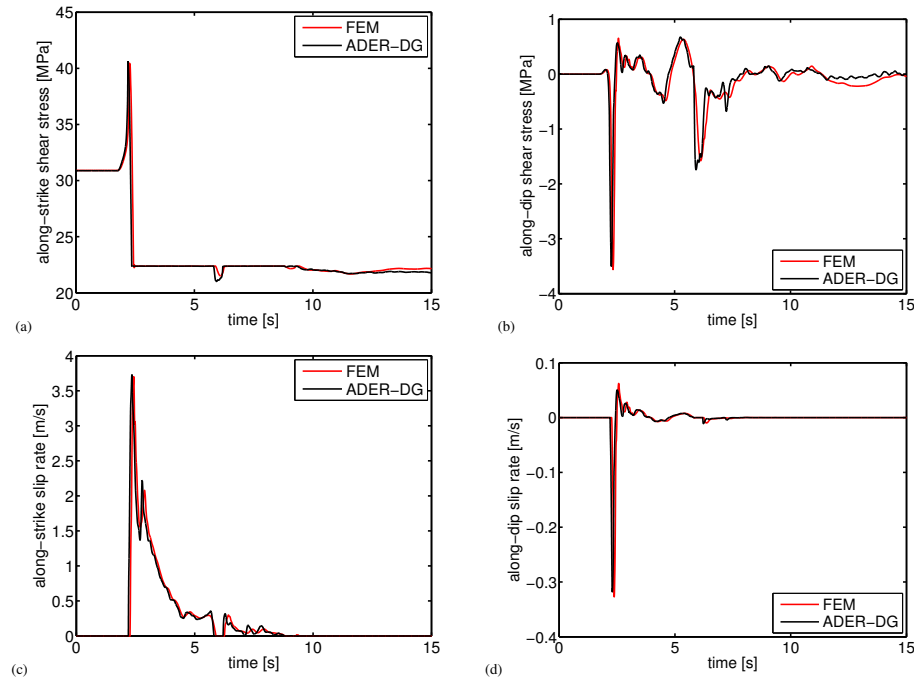


Fig. 6. Shear stresses and slip rates for TPV17 at receiver located 9 km deep and 9 km along strike. The ADER-DG solution is shown in black, the FEM comparison solution in red.

Title Page

Abstract

Introduction

Conclusions

References

Tables

Figures

◀

▶

◀

▶

Back

Close

Full Screen / Esc

Printer-friendly Version

Interactive Discussion



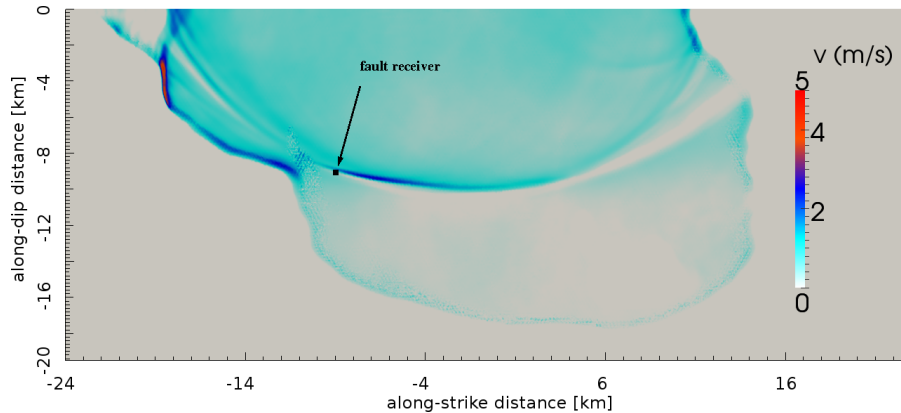


Fig. 7. Horizontal slip rate v in m s^{-1} for TPV17 at $t = 5.5$ s, the moment when the interface wave which originated at the free surface approaches the fault receiver shown in Fig. 5, indicated by the arrow. The elliptical shape of the interface wave, which consists of a healing phase followed by a high slip rate front, is clearly visible.

Verification of an ADER-DG method

C. Pelties et al.

Title Page

Abstract Introduction

Conclusions References

Tables Figures

◀ ▶

◀ ▶

Back Close

Full Screen / Esc

Printer-friendly Version

Interactive Discussion



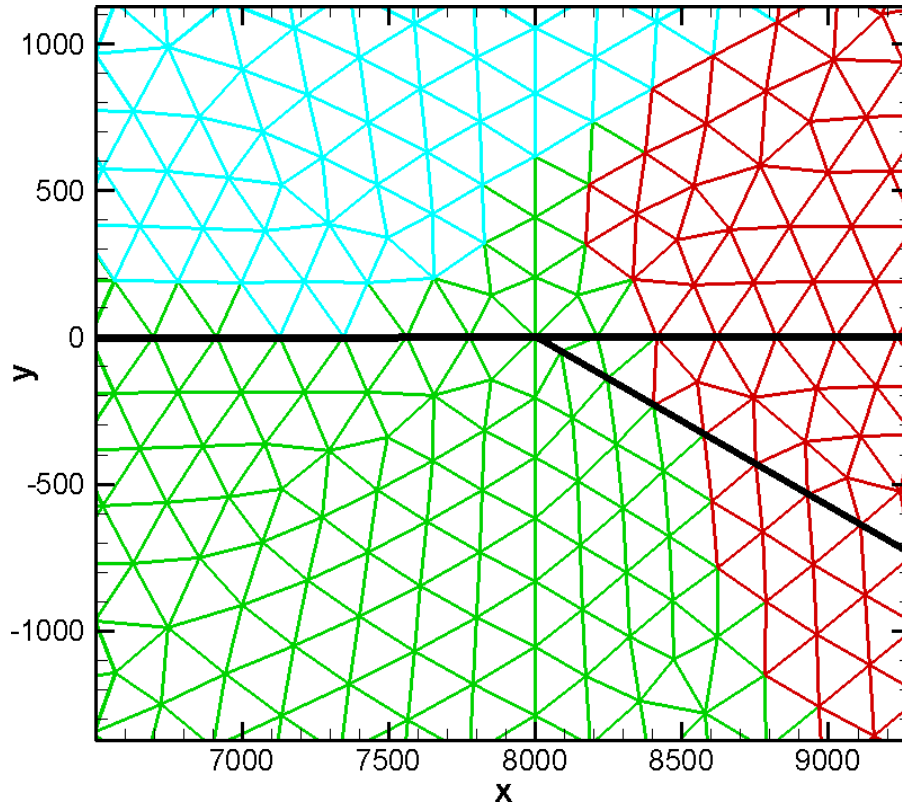


Fig. 8. Zoom view of the junction point of TPV15 (2-D example) to illustrate parallelization concept and discretization strategy.

GMDD

6, 5981–6034, 2013

Verification of an ADER-DG method

C. Pelties et al.

Title Page	
Abstract	Introduction
Conclusions	References
Tables	Figures
◀	▶
◀	▶
Back	Close
Full Screen / Esc	
Printer-friendly Version	
Interactive Discussion	



Verification of an
ADER-DG method

C. Pelties et al.

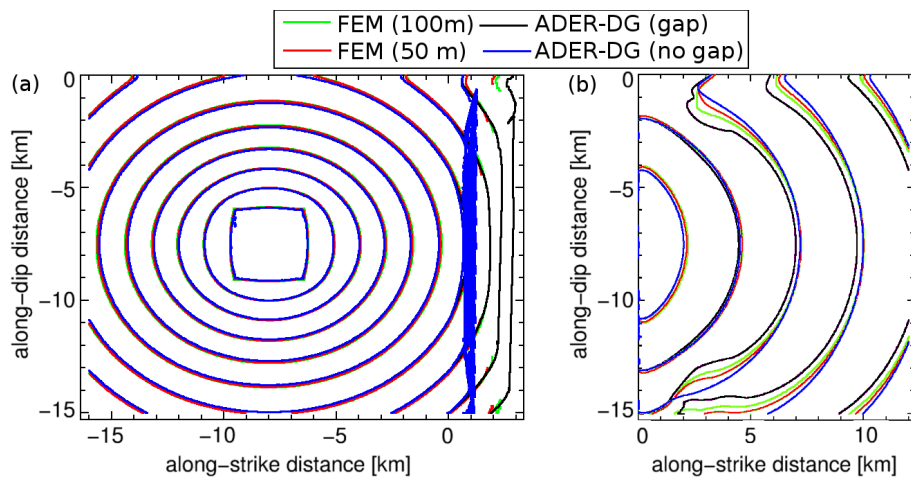


Fig. 9. Rupture contours in problem TPV15 on **(a)** the main fault and **(b)** the branch fault. ADER-DG solutions are shown in black (with gap) and blue (without gap), the FEM comparison solutions in red (50 m discretization) and green (100 m discretization).

[Title Page](#)[Abstract](#)[Introduction](#)[Conclusions](#)[References](#)[Tables](#)[Figures](#)[◀](#)[▶](#)[◀](#)[▶](#)[Back](#)[Close](#)[Full Screen / Esc](#)[Printer-friendly Version](#)[Interactive Discussion](#)

Verification of an ADER-DG method

C. Pelties et al.

Title Page

Abstract

Introduction

Conclusions

References

Tables

Figures

◀

▶

◀

▶

Back

Close

Full Screen / Esc

Printer-friendly Version

Interactive Discussion

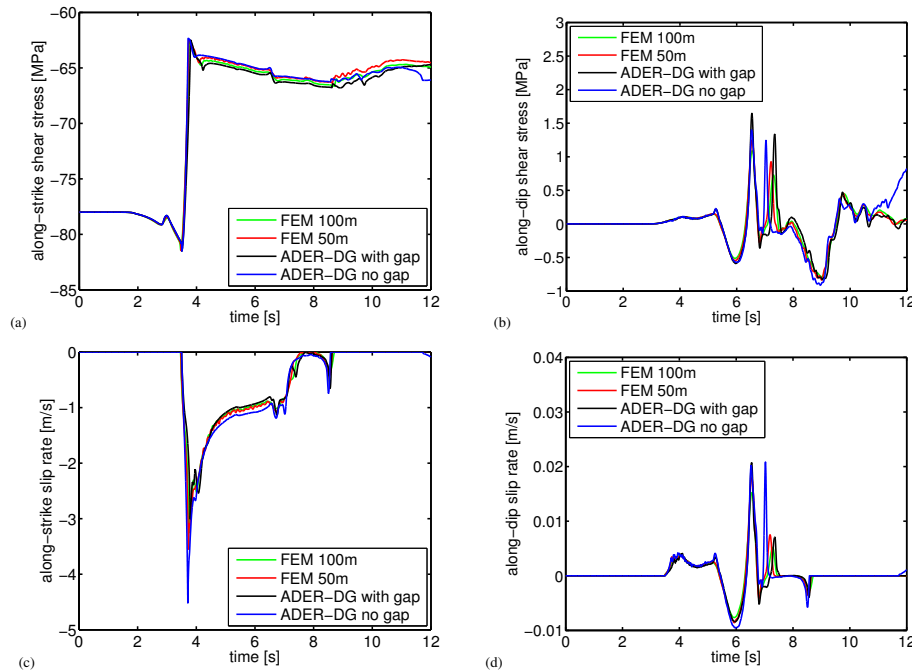


Fig. 10. Shear stresses and slip rates for TPV15 at a receiver located on the branch fault 9 km along-strike and 7.5 km deep. ADER-DG solutions are shown in black (with gap) and blue (without gap), the FEM comparison solutions in red (50 m discretization) and green (100 m discretization).

Verification of an ADER-DG method

C. Pelties et al.

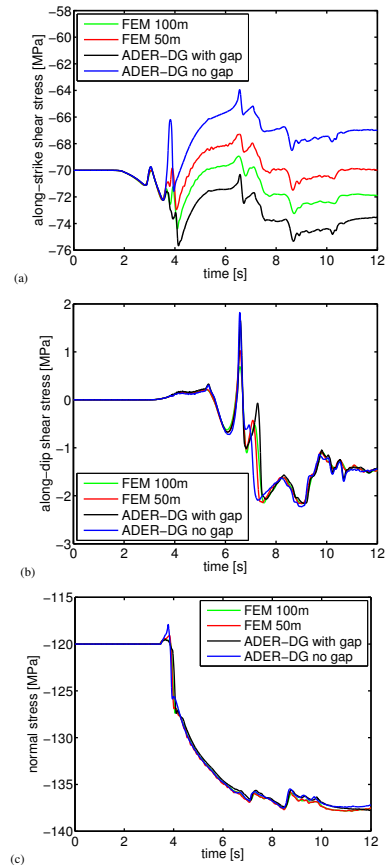


Fig. 11. Shear and normal stresses of TPV15 recorded 2 km before the junction point and 7.5 km deep. Differences are due to differences in geometrical setups as discussed in the main text. ADER-DG solutions are shown in black (with gap) and blue (without gap), the FEM comparison solutions in red (50 m discretization) and green (100 m discretization).

[Title Page](#)
[Abstract](#)
[Introduction](#)
[Conclusions](#)
[References](#)
[Tables](#)
[Figures](#)
[◀](#)
[▶](#)
[◀](#)
[▶](#)
[Back](#)
[Close](#)
[Full Screen / Esc](#)
[Printer-friendly Version](#)
[Interactive Discussion](#)


Verification of an
ADER-DG method

C. Pelties et al.

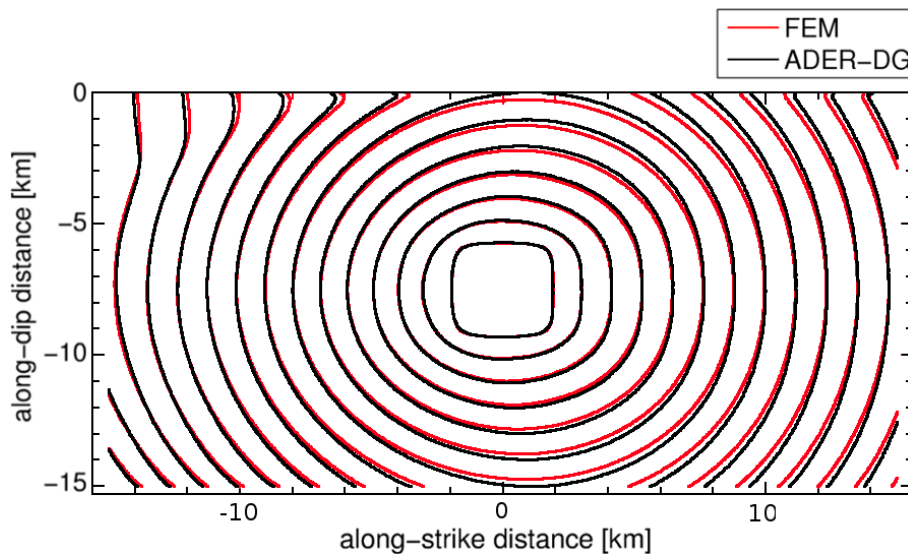


Fig. 12. Rupture front every 0.5 s in problem TPV6 with bi-material conditions. The ADER-DG solution is shown in black, the FEM comparison solution in red.

[Title Page](#)[Abstract](#)[Introduction](#)[Conclusions](#)[References](#)[Tables](#)[Figures](#)[◀](#)[▶](#)[◀](#)[▶](#)[Back](#)[Close](#)[Full Screen / Esc](#)[Printer-friendly Version](#)[Interactive Discussion](#)

Verification of an
ADER-DG method

C. Pelties et al.

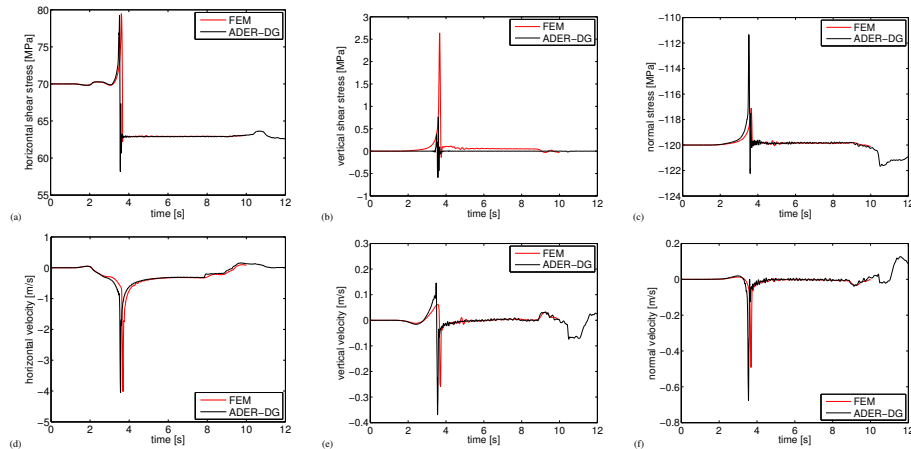


Fig. 13. Stresses and velocities of TPV6 at a surface station located on the near side of the fault at 0 km along-strike. The ADER-DG solution is shown in black, the FEM comparison solution in red.

Title Page

Abstract

Introduction

Conclusions

References

Tables

Figures

⏪

⏩

◀

▶

Back

Close

Full Screen / Esc

Printer-friendly Version

Interactive Discussion



Verification of an ADER-DG method

C. Pelties et al.

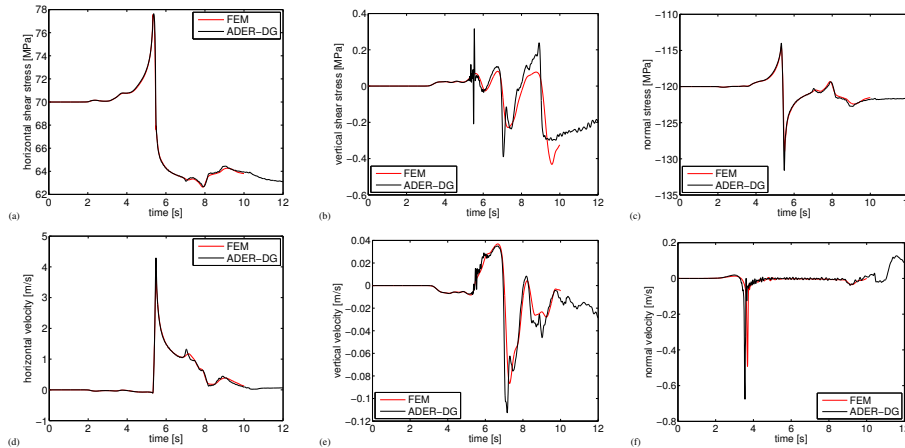


Fig. 14. Stresses and velocities of TPV6 at a station located on the far side of the fault – 12 km along-strike and 7.5 km deep, which corresponds to the hypocenter depth. The ADER-DG solution is shown in black, the FEM comparison solution in red.

Title Page

Abstract

Introduction

Conclusions

References

Tables

Figures

⏪

⏩

◀

▶

Back

Close

Full Screen / Esc

Printer-friendly Version

Interactive Discussion



Verification of an
ADER-DG method

C. Pelties et al.

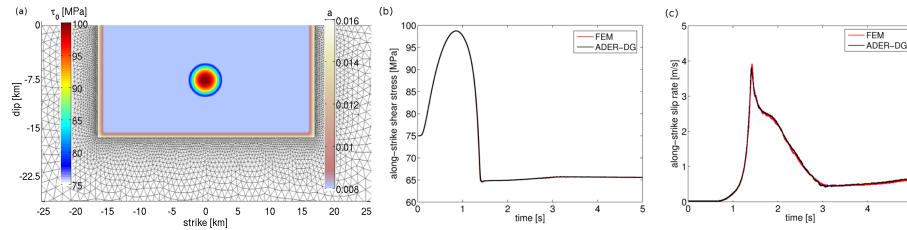


Fig. 15. (a) Nucleation and initial frictional parameters of SCEC TPV101. A velocity weakening fault smoothly transitions to a surrounding velocity-strengthening material, by adapting the frictional parameter a . Nucleation is achieved by prescribing a space and time dependent circular stress perturbation. Along-strike (b) shear stress and (c) slip rate during nucleation at the hypocenter, located at 0 km along strike and 7.5 km along dip. The ADER-DG solution is shown in black, the FEM comparison solution in red.

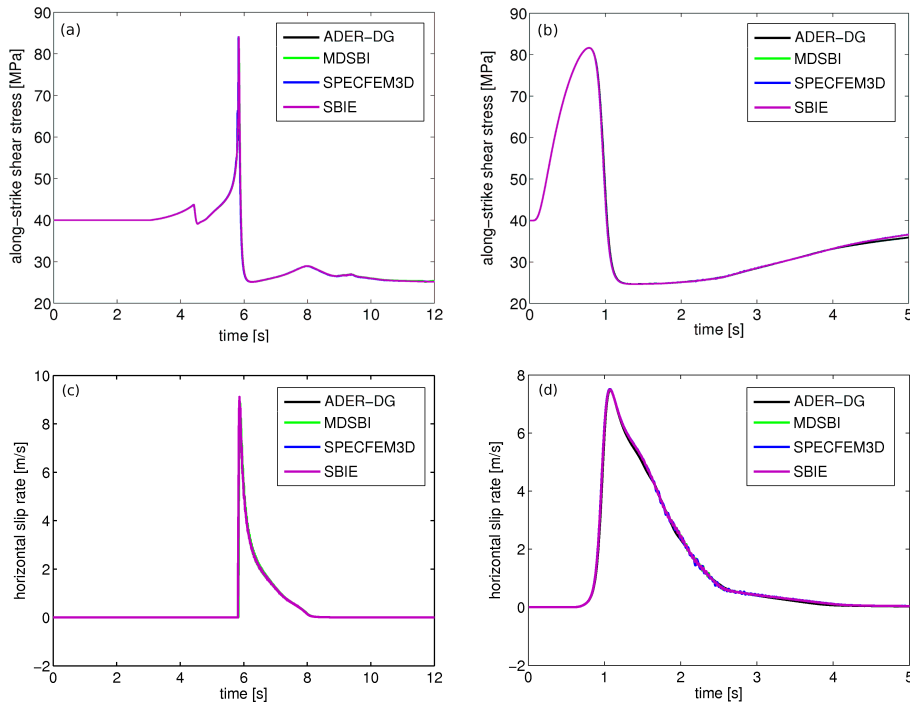


Fig. 16. Fast velocity weakening benchmark TPV103 results. Comparison of ADER-DG (black) with the high-order dynamic rupture software packages MDSBI (Dunham, 2008), SPECFEM3D (Kaneko et al., 2008) and SBIE (Lapusta and Liu, 2009). Along-strike **(a)** shear stress and **(c)** slip rate on the fault at 12 km along strike and 3 km along dip. Along-strike **(b)** shear stress and **(d)** slip rate during nucleation at the hypocenter at strike 0 km, dip 7.5 km. The ADER-DG solution is shown in black, the comparison solutions of MDSBI in green, SPECFEM3D in blue and SBIE in purple.

Verification of an ADER-DG method

C. Pelties et al.

[Title Page](#)

[Abstract](#) [Introduction](#)
[Conclusions](#) [References](#)
[Tables](#) [Figures](#)

⏪ ⏩
◀ ▶
[Back](#) [Close](#)

[Full Screen / Esc](#)

[Printer-friendly Version](#)

[Interactive Discussion](#)



Verification of an
ADER-DG method

C. Pelties et al.

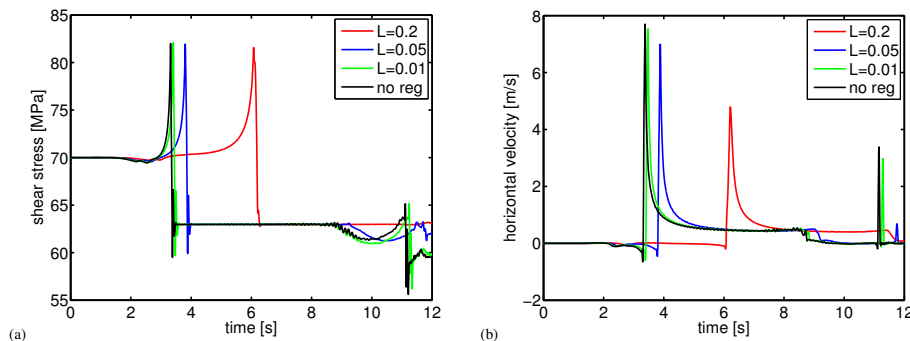


Fig. 17. Influence of Prakash–Clifton regularization on ADER-DG solution of the ill-posed bi-material problem TPV7. Time series at a surface receiver located on the far side off the fault above the nucleation zone, for different values of the characteristic regularization length scale L .

[Title Page](#)[Abstract](#)[Introduction](#)[Conclusions](#)[References](#)[Tables](#)[Figures](#)[⏪](#)[⏩](#)[◀](#)[▶](#)[Back](#)[Close](#)[Full Screen / Esc](#)[Printer-friendly Version](#)[Interactive Discussion](#)